Sliding Response Under Multi-Component Excitation

EFFECT OF MULTI-COMPONENT EXCITATION ON THE SLIDING RESPONSE OF UNANCHORED COMPONENTS IN NUCLEAR FACILITIES

By

AAMNA ARSHAD, B.ENG

Faculty of Engineering

Department of Civil Engineering

A Thesis Submitted to the School of Graduate Studies in Partial Fulfillment of the Requirements for the Degree Master of Applied Science

McMaster University

Master of Applied Science (2019) McMaster University

(Civil Engineering) Hamilton, Ontario

TITLE	Effect of Multi-Component Excitation on the Sliding Response of Unanchored Components in Nuclear Facilities
AUTHOR	Aamna Arshad, B.Eng
SUPERVISOR	Dr. Michael Tait
ADJUNCT SUPERVISOR	Dr. Dimitrios Konstantinidis
NUMBER OF PAGES	90 pages (xvi, 74)

To my family and friends

Lay Abstract

Earthquakes can pose a huge risk to nuclear facilities. Unanchored objects within the facility may collide and interact with safety-critical equipment. Previous research on sliding behaviour lacks information on the response of an object subjected to earthquake excitation in both the horizontal plane and vertical direction simultaneously. Several prediction equations and an approximate method have been developed to estimate the sliding response as it becomes computationally expensive to solve. This research investigates the influence of simulatenous multi-component excitation on the sliding behaviour and evaluates the current standardized approximate method of estimating sliding displacement. Recommendations are given based on the friction coefficient between the object and the base. The research also explores which characteristics of earthquake ground motion (e.g. acceleration, velocity, energy) are most indicative of sliding behaviour.

Abstract

During an earthquake, unanchored equipment within a nuclear power plant facility can slide and interact with safety-critical systems and components. Previous studies on sliding have largely focused on the response due to unidirectional excitation, as computing the response of unanchored components in three dimensions can be complex and computationally expensive. As such, several prediction equations and a standardized approximate method as outlined in ASCE 4-16 have been developed to estimate the peak sliding displacement. This study investigates the effect of bidirectional horizontal interaction and the influence of vertical excitation on the sliding response of an unanchored object when the x, y, and z, components of earthquake excitation are applied simultaneously. The study also evaluates the approximate method detailed in ASCE 4-16. A suite of 40 floor acceleration histories obtained from response history analysis of a representative nuclear power plant facility are used as input for the sliding model. A wide range of friction coefficients is selected for analysis and the nonlinear sliding response of components is determined through the use of a Bouc-Wen type hysteretic model. Computed responses under uni-, bi- and tri-directional excitation reveal that the effect of bidirectional interaction and vertical excitation is greatest for sites with high shaking intensity. It is also concluded that the ASCE 4-16 approximate method is significantly overconservative in all cases. Additionally, the study expands the concept of multi-component excitation to intensity measures. Twelve intensity

measures are selected and evaluated. It is found that most efficient intensity measures vary in efficiency depending on the coefficient of friction, and that the top intensity measures are not significantly affected by incorporating multiple components of excitation.

Acknowledgements

I am deeply grateful to Dr. Michael Tait for his guidance towards the completion of this thesis. I would also like to sincerely thank Dr. Wael El-Dakhakhni and Dr. Ahmad Siam for their support within the CaNRisk-CREATE program and encouragement during challenging times.

Table of Contents

List of Tables

List of Figures

List of Abbreviations and Initialisms

A_{RMS}	Root Mean Square Acceleration
CAV_{exc}	Cumulative Absolute Velocity of Exceedance
EC	Equipment and Contents
EDP	Engineering Demand Parameter
HGBW	Harvey and Gavin Bouc-Wen
I_A	Arias Intensity
I_C	Characteristic Intensity
I_F	Fajfar Index
IM	Intensity Measure
NPP	Nuclear Power Plant
PGA	Peak Ground Acceleration
PFA	Peak Floor Acceleration
PFV	Peak Floor Velocity
PFD	Peak Floor Displacement
SRSS	Square-Root of the Sum of the Squares
t_{brc}	Bracketed Duration
t_{sig}	Significant Duration
t_{uni}	Uniform Duration

Declaration of Academic Achievement

The work presented in this thesis represents original research that Aamna Arshad conducted under the technical supervision of Dr. Dimitrios Konstantinidis. When Dr. Konstantinidis left McMaster University in January 2019, Dr. Michael Tait was asked to take over the role of supervisor, while Aamna continued to work on research with Dr. Konstantinidis. Dr. Tait reviewed the thesis and provided editorial comments. Aamna provided ground motion input to Mohammadreza Najafi (MASc Student, McMaster University) who analyzed the NPP model in OpenSees to provide floor acceleration histories. Specific research contributions are listed below.

Aamna Arshad's contributions in this research include the following:

- Selected the location of the sites and assessed their seismic hazard
- Selected and scaled ground motion suites for the two sites
- Coded the model in MATLAB
- Verified the model against numerical and experimental results
- Carried out all response history analysis of sliding components
- Selection and evaluation of intensity measures
- Prepared all figures in the thesis
- Analyzed and interpreted the results
- Prepared first complete draft and revised subsequent drafts based on detailed feedback (both technical and editorial) by Dr. Konstantinidis

Dimitrios Konstantinidis' contributions in this research include the following:

- Defined the research topic, objectives, and scope
- Proposed the type of model and analysis method to be used
- Facilitated collaboration to get the nuclear power plant floor motions from his student Mr. Mohammadreza Najafijozani
- Proposed the investigation of the bidirectional excitation on the sliding response
- Proposed the study of the effect of vertical excitation
- Proposed the evaluation of the approximate method in ASCE 43-05 and 4-16 for sliding components
- Proposed the evaluation of spatial combination rules for the sliding problem
- Gave specific direction for the presentation of the research results (floor acceleration spectra, displacement orbits, sliding spectra)
- Gave specific direction for the evaluation of best intensity measures for sliding components
- Proposed the investigation of intensity measures that consider multiple components of excitation
- Provided significant editing, reorganization, and writing of parts of Chapter 2.

Chapter 1. Introduction

1.1 Motivation

Nuclear power generation is a key component of clean sustainable energy to meet the world's growing energy demands. Large economies such as China and India have recently committed to accelerating their clean energy production, such as solar, wind and nuclear power generation [1]. Nuclear power was responsible for producing 15% of Canada's energy needs in 2017 [2]. Currently, the United States has the largest output of nuclear energy and operates the most number of nuclear power plants (NPPs) in the world. Ninety-nine nuclear generators provide 20% of the country's energy needs [3]. In addition to power generation, nuclear reactors also produce isotopes with applications in medicine and industry.

Following the Fukushima-Daichi disaster in 2011, many countries and governing agencies tightened their standards for nuclear safety and re-evaluated their existing nuclear generating facilities that were under risk from natural disasters. In the United States, the nuclear regulatory commission (NRC) required all NPPs to conduct a comprehensive flooding and earthquake hazard analysis [4]. Post-Fukushima, seismic walkdowns of U.S. power plant sites identified potential interactions of non-structural components during an earthquake and possible issues with temporary installations and portable equipment [5].

The impact and importance of non-structural components is well-documented following the 1994 Northridge earthquake. After the earthquake, non-structural damage from seismic events resulted in hospitals, businesses and industrial facilities to become inoperable even when there was little-to-no structural damage [6]. Figure 1.1.1 shows the aftermath inside an office at the University of Canterbury following the 2010 Christchurch Earthquake. The institution was closed for over a week to assess damage from nonstructural components [7]. Non-structural failure routinely accounts for the majority of earthquake damage in the developed world, as buildings are increasingly employing new and expensive or fragile equipment that may be unrestrained [8]. FEMA E-74 [8] classifies non-structural components into three groups: 1) architectural 2) mechanical, electrical and plumbing, and 3) furniture, equipment or contents. The majority of architectural components such as partitions, glazing and cladding are often anchored or bonded to structural components.

Figure 1.1.1 University of Canterbury in New Zealand following the 2010 Christchurch Earthquake [7]

This study will focus specifically on equipment and contents (EC) which can be unanchored and free to slide and interact with other systems. While typically nuclear standards state that EC should be restrained in NPP facilities, unanchored EC are permitted provided that the ASCE 43-05 provisions are satisfied [9]. There is still a need for unanchored equipment within the plant for practicality or mobility reasons. Typical examples of unanchored EC in nuclear facilities are: computer equipment, tool cabinets, water tanks, storage vessels, rolling platforms/ scaffolding, transformers, hand carts and used fuel containers [10]. Equipment which can be classified as 'stocky' as opposed to slender is more likely to slide. This unanchored equipment can potentially slide and interact with safety-critical systems during a seismic event. Reports from the Fukushima disaster following the Tohoku Earthquake in 2011 indicate that there were instances of toppling of unanchored equipment within the nuclear facilities [11]. In one instance, a locking device was broken due to the sliding motion of a hatch on rails.

In general, the damage inflicted on the structural and other non-structural components by the movement of unanchored equipment can pose a safety risk, as identified by the NRC seismic walkdowns. The main risks associated with damage to non-structural components are: life safety, property loss and interruption/loss of essential functions. For power-generation facilities, such as NPPs, the consequences of damage to non-structural components can be far-reaching. Extra care needs to be taken when restraining equipment, and accurate methods are important for modelling or predicting the movement of unrestrained equipment.

Often the sliding analysis of components due to multi-directional excitation can be complex or computationally expensive; hence the need for approximate procedures and analysis.

1.2 Mechanics of Sliding

The mechanics of sliding for a rigid block are dependent on the inertial forces acting on the block, $\ddot{u}$, and the coefficient of friction between the rigid block and base, μ. In this study, it is assumed that Coulomb friction will represent the behaviour at the contact interface. The maximum value that that the force of friction can attain during the non-sliding phase is $F_f = \mu_s m(g + \ddot{u}_{fx})$. However, when the block is sliding the friction force is equal to:

$$F_f = \mu m(g + \ddot{u}_{fz}) \tag{1}$$

Based on Figure 1.2.1, analyzing the horizontal forces and normalizing by mass results in the equation of motion (2).

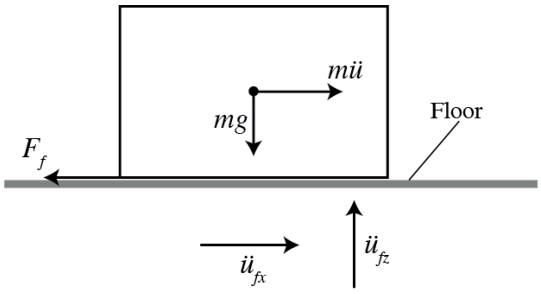

Figure 1.2.1 Unanchored rigid sliding block under horizontal and vertical excitation

Note that the direction of friction force is dependent on the direction of the block's velocity, $\dot{u}_x$. This is represented using the signum function where a positive value for $\dot{u}_x$ returns 1, and a negative value returns -1.

$$\ddot{u}_x + \left[\mu\left(g + \ddot{u}_{fz}\right)\right]\text{sgn}(\dot{u}_x) = -\ddot{u}_{fx} \tag{2}$$

1.3 Background

In 1996, Shenton [12] categorized the five major response modes for unanchored objects: rest, slide, rock, slide-rock, and lift off. The most common response mode for stockier objects is sliding. Stockiness is defined by the ratio of the object's width to its height. Assuming that the unanchored objects can be modelled as blocks, the block's first mode response is dependent on the width to height ratio (*B/H*), coefficient of static friction μ_s, and the peak ground acceleration A_g (g). Typically, the initial mode of response from rest predicts the subsequent behaviour of the block. Shenton categorized the criteria for the initiation of the sliding mode of a rigid block. Considering the case where $A_g < B/H$, the sliding mode will continue to govern until $A_g < \mu_s$. At this point, the ground acceleration is not sufficient to surpass the frictional force and there is no sliding. For cases where $B/H < A_g$, the slide mode will continue to govern until $\mu_s = B/H$. Increasing the friction coefficient beyond *B/H* will result in the slide-rock or rocking movement. The two response modes considered for the study in Chapter 2 are rest and sliding.

Under Coulomb friction, which assumes rigid-perfectly-plastic behaviour, the sliding response will be initiated for the block when the excitation surpasses the friction force, μmg. This idealized behaviour is shown in Figure 1.3.1.

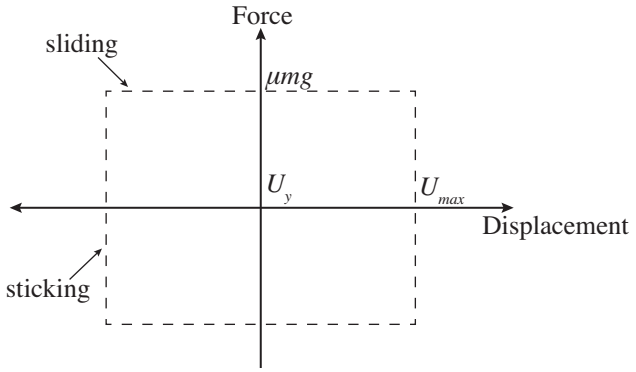

Figure 1.3.1 Hysteretic sliding behaviour of a rigid block under unidirectional excitation

The initiation criteria for sliding in the presence of vertical excitation was discussed by Lopez Garcia and Soong [15]. Simply, the sliding movement is initiated instead of rocking when the horizontal inertial forces acting on the block are larger than the restoring moment due to the weight of the block and vertical acceleration. This simplifies to the criteria:

$$\frac{B}{H} \geq \frac{|\ddot{u}_{fx}|}{g+\ddot{u}_{fz}} \tag{3}$$

1.3.1 Sliding

There has been some effort over the years to better understand sliding behaviour in both structural and non-structural components subjected to single or multi-directional excitation. Jangid [13] investigated the seismic response of a structure on a sliding base due to bidirectional earthquake excitation and determined that the sliding displacement is increased under bidirectional (*x* and *y*)

excitation due to the interaction of friction forces. The study concluded that sliding displacement may be underestimated from analysis of only single-component excitation. Regarding nonstructural components, Choi and Tung [14] estimated the sliding displacement of unanchored bodies subjected to unidirectional earthquake excitation based on Newmark's solution for the maximum sliding displacement of a rigid block subjected to a rectangular acceleration pulse. Regarding the effect of vertical excitation, Lopez Garcia and Soong [15], and Farzad and Konstantinidis [16] have both considered the effect of vertical excitation on the behaviour of sliding objects, but only within unidirectional sliding models.

When it comes to modelling sliding displacement, which is mainly dependent on the force of friction – numerous friction models exist in the area of tribology that can accurately model the friction force. Basic models include simple Coulomb, Coulomb + static, or Stribeck friction which considers the velocity dependence of friction. More detailed friction models, such as the Dahl model, can capture the slight deformation in the contact surfaces before sliding occurs, also known as pre-sliding motion or the break-away phenomenon. There are also more complex models such as the LuGre, Leuven and seven-parameter friction models which incorporate the Stribeck effect and viscous friction with the Dahl model [17]. However, these models require numerous parameters to calibrate effectively, and it can be difficult to accurately estimate these parameters. The type of data that these models require has not yet been aggregated for sliding objects, specifically regarding the nonstructural contact interfaces typically found in a NPP.

To identify these friction parameters would require significant work. Previously conducted experimental studies on pull tests of heavy equipment by Konstantinidis and Makris [18] assumed static + Coulomb or Coulomb friction. Testing of sliding bench-top equipment for performance characterization by Chaudhuri and Hutchinson [19] [20] also only reported the static and kinetic friction coefficients. With the exception of Nikfar and Konstantinidis [21] who modelled Stribeck friction, to capture the stick-slip phenomenon of sliding, many studies estimating the sliding response of building EC have employed a Coulomb friction model. These include: Choi and Tung [14], Lopez Garcia and Soong [15], Konstantinidis and Makris [18] [22], and Konstantinidis and Nikfar [23].

Furthermore, the Dahl, LuGre, Leuven friction models are primarily for unidirectional movement and do not include the bidirectional interaction of friction forces. Therefore the use of these complex friction models is not ideal for the investigation in Chapter 2.

Contrastingly, Bouc-Wen type models have been expanded to include bidirectional excitation. Bouc-Wen models are based on a differential equation which includes parameters that can be calibrated to modify the shape of the hysteresis and can be used to model a variety of behaviour, including friction. This class of models has been favoured when modelling the hysteretic behaviour of friction pendulum bearings, elastomeric bearings and other complex hysteretic devises such as magneto-rheological dampers. They rely on experimental hysteretic

data for accurate calibration of the parameters γ, β, and η to replicate realistic hysteresis.

The first uniaxial model was originally developed by Bouc in 1967 and extended by Wen in 1976 [24]. The dimensionless hysteretic quantity, z, and the displacement, u, is determined by solving the following:

$$\dot{z} = \frac{1}{U}[\dot{u} - \beta|\dot{u}|\, z\, |z|^{\eta-1} - \gamma\dot{u}|z|^{\eta}] \tag{1}$$

where U is the yield displacement, β and γ are parameters that describe the shape of the hysteresis and η is the knee sharpness which controls how sharp the transition is from elastic to plastic behaviour [24]. The restoring force is a function of the displacement response and hysteretic quantity, z.

The model was expanded upon in 1986 by Park et al. [25] to include biaxial interaction in order to model the response of reinforced concrete columns that were significantly affected by biaxial structural interaction in the plastic range. Park et al. expanded the model to be bidirectional by proposing two coupled differential equations; the hysteretic components, z_x and z_y in both orthogonal directions are determined by solving a pair of coupled differential equations. This model was also used by Nagarajaiah et al. [26] to model the non-linear behaviour of elastomeric and sliding isolation bearings supporting a six-story reinforced concrete structure.

In 2000, Wang and Wen [27] further developed the Park-Wen model for biaxial hysteresis by extending the governing equations for any value of η. This

model has been used to analyze connection failure in steel buildings under multidirectional earthquake excitation. However, this generalization affected the rotational invariance of the model and it was no longer isotropic for values of $\eta > 2$, such that the hysteretic behaviour varied along different directions. Following this investigation, Harvey and Gavin [28] proposed a model that was biaxial and also isotropic for all values of η. While these models have primarily been used to accurately model the hysteretic behaviour of different types of isolators through calibration of the γ, β, η parameters – they can also be used to model sliding behaviour of a rigid object under Coulomb friction by fixing the yield displacement to be near zero. In general, Bouc-Wen type models represent a black box approach to modelling frictional sliding behaviour in the sense that they can replicate realistic behaviour by calibrating the parameters to match experimental output data, given the same input.

Parallel to this, there has also been development of several prediction equations to estimate sliding displacement due to earthquake excitation. The first being Newmark's [29] initial equation for the estimation of sliding behaviour of a block resting on the ground which is subjected to a rectangular acceleration pulse in 1965. Newmark theorized that the sliding displacement was a function of the peak ground velocity and acceleration. Kaneko et al. [30] proposed the first empirical equation for estimating sliding which was based on absolute floor velocity. Choi and Tung [14] modified Newmark's original equation to include peak ground displacement instead of velocity. Following experimental tests,

Konstantinidis and Makris [18] proposed an equation where the sliding displacement is calculated as a function of peak floor acceleration and the angular frequency of the predominant pulse in the floor acceleration. Most recently, Yeow et al. [31] proposed a lengthy prediction equation dependent on absolute floor velocity and *R* a ratio of the coefficient of friction and absolute floor acceleration.

Another popular method for predicting sliding displacement was introduced in ASCE 43-05 [9] as an allowable approximate method to estimate sliding behaviour in lieu of nonlinear analysis. By virtue of being codified, it is also the most commonly used method for approximating peak sliding displacement in engineering practice. The method requires the engineers to first calculate a reduced friction coefficient, which is dependent on the peak vertical acceleration. The method also requires the determination of the lowest natural frequency at which the horizontal spectral acceleration equals the sliding coefficient, which is a function of the reduced friction coefficient. This approximate method was also reiterated in ASCE 4-16 [32], making it the current standard for estimating peak sliding displacement.

1.3.2 Intensity Measures

Intensity measures (IMs) were introduced as a way to link the behaviour of the structure with seismic characteristics of the ground motion; examples of which include: magnitude, distance and fault-type. IMs should include sufficient information about the earthquake so that the structural (or in this case, nonstructural) response can be estimated efficiently. The identification of proper

IMs is also instrumental in the performance-based earthquake engineering framework where identifying the correct IMs is the first step to developing fragility curves. In this context, fragility curves can be used to determine the probability of EC exceeding a certain sliding displacement limit.

The most common example of an IM is peak ground acceleration (PGA), which is used in United States Geological Survey (USGS) seismic maps as a measure of shaking intensity. PGA is also directly related to the inertial forces that buildings experience. There has been considerable work on identifying new and better IMs to better predict building response – including bivariate or vector intensity measures that are a combination of two or more individual IMs [33][34]. However, there has not been much investigation in including all three components of the ground motion excitation in the x, y and z directions and its effect on IM efficiency. There has been some initial investigation on IMs for sliding displacement by Konstantinidis and Nikfar [35], and Konstantinidis and Makris [18][22] who proposed a dimensionless IMs for predicting sliding displacement in base-isolated and fixed-base buildings, respectively. Nikfar and Konstantindis have also developed fragility curves for unanchored medical equipment on casters [36][37]. However, significantly more research has been done on the best IMs for rocking structures and rocking non-structural components as investigated by Giouvanidis and Dimitrakopoulos [34][38], and Dimitrakopoulos and Paraskeva [33] . Currently, there has not been any investigation of multiple intensity measures with respect to sliding behaviour.

1.4 Research Objectives and Scope

Based on the safety risk of unanchored EC in NPPs and lack of knowledge on the best intensity measures for sliding, this research will investigate the sliding behaviour of non-structural components within NPPs under seismic excitation, with specific consideration to:

- The influence of bidirectional interaction of friction forces and the vertical component of acceleration on sliding displacement.
- Accuracy of the ASCE 4-16 approximate method and spatial combination rules.
- Comparison of various intensity measures with respect to sliding displacement and changes in their accuracy due to incorporating multi-component excitation.

The key assumptions in this research are:

- The friction coefficient between the floor and EC in NPPs as well as the height to width ratio of EC are conducive to sliding.
- The EC and floor are both rigid and do not deform under earthquake excitation.
- The behaviour of the EC and internal structure of the NPP are uncoupled.

1.5 Thesis Outline

Chapter 1 of this thesis presents the motivation, background information and literature review of previous study on sliding behaviour due to earthquake

excitation. Chapter 2 focuses on meeting the research objectives outlined in Section 1.4 and has been prepared as a manuscript to be submitted to the *Journal of Earthquake Engineering and Structural Dynamics.* Chapter 3 summarizes the results and recommendations from the research conducted in Chapter 2 and also provides suggestions for future investigation.

1.6 References

1. Allianz Climate Solutions. China and India Lead Global Renewable Energy Transition. *United Nations Climate Change* 2017. https://unfccc.int/news/china-and-india-lead-global-renewable-energy-transition [accessed February 17, 2019].
2. Nuclear Power in the World Today. *World Nuclear Association* 2019. http://www.world-nuclear.org/information-library/current-and-future-generation/nuclear-power-in-the-world-today.aspx [accessed February 17, 2019].
3. International Atomic Energy Agency (IAEA). Nuclear Share of Electricity Generation in 2017. *IAEA: Power Reaction Information System* 2017. https://pris.iaea.org/PRIS/WorldStatistics/NuclearShareofElectricityGeneration.aspx [accessed February 17, 2019].
4. USNRC. Backgrounder on NRC Response to Lessons Learned from Fukushima. *United States Nuclear Regulatory Comission* 2018. https://www.nrc.gov/reading-rm/doc-collections/fact-sheets/japan-events.html [accessed February 18, 2019].
5. Flanders S, Chokshi N, Bensi M, Munson C, Cook C, Campbell A, *et al.* Insights Gained from Post-Fukushima Review of Seismic and Flooding Hazards at Operating U.S. Nuclear Power Plant Sites, *24th Conference on Structural Mechanics in Reactor Technology - SMiRT 24*. Busan, South Korea: 2017.
6. Todd D, Carino N, Chung R, Lew HS, Taylor A, Walton W, *et al. 1994 Northridge Earthquake: Performance of Structures, Lifelines, and Fire Protection Systems*. National Institute of Standards Technology (NIST); .
7. Marion Lloyd. 2 Universities in New Zealand Cope With Earthquake Damage. *The Chronicle of Higher Education* 2010.
8. Wiss, Janney, Elstner Associates, Inc. *FEMA 74 - Reducing the Risks of Nonstructural Earthquake Damage: A Practical Guide*. vol. 74. 3rd ed. FEMA; 1994.

9. ASCE. *ASCE 43-05: Seismic Design Criteria for Structures, Systems, and Components in Nuclear Facilities*. Reston, VA: American Society of Civil Engineers; 2005. DOI: 10.1061/9780784407622.
10. Dar A. Evaluation of Seismic Design Criteria for Rocking Objects in Nuclear Facilities. *MASc*. McMaster University, 2014.
11. IAEA. *IAEA Mission to Onagawa Nuclear Power Station to Examine the Performance of Systems, Structures and Components Following the Great East Japanese Earthquake and Tsunami*. Onagawa and Tokyo, Japan: 2012.
12. Shenton III HW. Criteria for Initiation of Slide, Rock, and Slide-Rock Rigid-Body Modes. *Journal of Engineering Mechanics* 1996; **122**(7): 690–693. DOI: 10.1061/(ASCE)0733-9399(1996)122:7(690).
13. Jangid RS. Seismic response of sliding structures to bidirectional earthquake excitation. *Earthquake Engineering & Structural Dynamics* 1996; **25**(11): 1301–1306. DOI: 10.1002/(SICI)1096-9845(199611)25:11<1301::AID-EQE618>3.0.CO;2-3.
14. Choi B, Tung CCD. Estimating Sliding Displacement of an Unanchored Body Subjected to Earthquake Excitation. *Earthquake Spectra* 2002; **18**(4): 601–613. DOI: 10.1193/1.1516750.
15. Lopez Garcia D, Soong TT. Sliding fragility of block-type non-structural components. Part 1: Unrestrained components. *Earthquake Engineering & Structural Dynamics* 2003; **32**(1): 111–129. DOI: 10.1002/eqe.217.
16. Nikfar F, Konstantinidis D. Peak Sliding Demands on Unanchored Equipment and Contents in Base-Isolated Buildings under Pulse Excitation. *Journal of Structural Engineering* 2017; **143**(9): 04017086. DOI: 10.1061/(ASCE)ST.1943-541X.0001811.
17. Liu YF, Li J, Zhang ZM, Hu XH, Zhang WJ. Experimental comparison of five friction models on the same test-bed of the micro stick-slip motion system. *Mechanical Sciences* 2015; **6**(1): 15–28. DOI: 10.5194/ms-6-15-2015.
18. Konstantinidis D, Makris N. Experimental and analytical studies on the response of freestanding laboratory equipment to earthquake shaking. *Earthquake Engineering & Structural Dynamics* 2009; **38**(6): 827–848. DOI: 10.1002/eqe.871.
19. Chaudhuri SR, Hutchinson TC. *Performance Characterization of Bench- and Shelf-Mounted Equipment*. UC Berkley: Pacific Earthquake Engineering Research Center; 2005.
20. Chaudhuri SR, Hutchinson TC. Fragility of Bench-Mounted Equipment Considering Uncertain Parameters. *Journal of Structural Engineering* 2006; **132**(6): 884–898. DOI: 10.1061/(ASCE)0733-9445(2006)132:6(884).
21. Nikfar F, Konstantinidis D. Effect of the Stick-Slip Phenomenon on the Sliding Response of Objects Subjected to Pulse Excitation. *Journal of Engineering Mechanics* 2017; **143**(4): 04016122. DOI: 10.1061/(ASCE)EM.1943-7889.0001183.
22. Konstantinidis D, Makris N. Experimental and analytical studies on the response of 1/4-scale models of freestanding laboratory equipment subjected to

strong earthquake shaking. *Bulletin of Earthquake Engineering* 2010; **8**(6): 1457–1477. DOI: 10.1007/s10518-010-9192-8.
23. Konstantinidis D, Nikfar F. Seismic response of sliding equipment and contents in base-isolated buildings subjected to broadband ground motions. *Earthquake Engineering & Structural Dynamics* 2015; **44**(6): 865–887. DOI: 10.1002/eqe.2490.
24. Wen YK. Method for random vibration of hysteretic systems. *Journal of the Engineering Mechanics Division* 1976; **102**(2): 249–263.
25. Park YJ, Wen YK, Ang AHS. Random vibration of hysteretic systems under bi-directional ground motions. *Earthquake Engineering & Structural Dynamics* 1986; **14**(4): 543–557. DOI: 10.1002/eqe.4290140405.
26. Nagarajaiah S, Reinhorn AM, Constantinou MC. Nonlinear Dynamic Analysis of 3-D-Base-Isolated Structures. *Journal of Structural Engineering* 1991; **117**(7): 2035–2054. DOI: 10.1061/(ASCE)0733-9445(1991)117:7(2035).
27. Wang CH, Wen YK. Evaluation of Pre-Northridge Low-Rise Steel Buildings. I: Modeling. *Journal of Structural Engineering* 2000; **126**(10): 1160–1168. DOI: 10.1061/(ASCE)0733-9445(2000)126:10(1160).
28. Harvey PS, Gavin HP. Truly isotropic biaxial hysteresis with arbitrary knee sharpness. *Earthquake Engineering & Structural Dynamics* 2014; **43**(13): 2051–2057. DOI: 10.1002/eqe.2436.
29. Newmark NM. Effects of Earthquakes on Dams and Embankments. *Géotechnique* 1965; **15**(2): 139–160. DOI: 10.1680/geot.1965.15.2.139.
30. Kaneko M. Evaluation of Sliding Displacement of Furniture during an Earthquake. *AIJ Journal of Technology and Design* 1999; **5**(8): 73–78. DOI: 10.3130/aijt.5.73.
31. Yeow TZ, MacRae GA, Dhakal RP, Lin SL. Predicting the Maximum Total Sliding Displacement of Contents in Earthquakes. *Journal of Architectural Engineering* 2016; **22**(1): 04015013. DOI: 10.1061/(ASCE)AE.1943-5568.0000193.
32. ASCE. *ASCE 4-16: Seismic Analysis of Safety-Related Nuclear Structures*. American Society of Civil Engineers; 2017.
33. Dimitrakopoulos EG, Paraskeva TS. Dimensionless fragility curves for rocking response to near-fault excitations. *Earthquake Engineering & Structural Dynamics* 2015; **44**(12): 2015–2033. DOI: 10.1002/eqe.2571.
34. Giouvanidis AI, Dimitrakopoulos EG. In Quest of Optimal Intensity Measures of Rocking Behaviour, *16th European Conference on Earthquake Engineering*. Thessaloniki: 2018.
35. Konstantinidis D, Nikfar F. Seismic response of sliding equipment and contents in base-isolated buildings subjected to broadband ground motions. *Earthquake Engineering & Structural Dynamics* 2015; **44**(6): 865–887. DOI: 10.1002/eqe.2490.
36. Nikfar F, Konstantinidis D. Seismic Performance of Hospital Equipment Supported on Wheels/Casters. *Earthquake Engineering & Structural Dynamics* 2017; **46**(2): 243–266. DOI: 10.1002/eqe.2789.

37. Nikfar F, Konstantinidis D. Experimental Study on the Seismic Response of Equipment on Wheels and Casters in Base-Isolated Hospitals. *Journal of Structural Engineering* 2019; **145**(3): 04019001. DOI: 10.1061/(ASCE)ST.1943-541X.0002266.
38. Giouvanidis AI, Dimitrakopoulos EG. Rocking amplification and strong-motion duration. *Earthquake Engineering & Structural Dynamics* 2018; **47**(10): 2094–2116. DOI: 10.1002/eqe.3058.

Chapter 2. Effect of Multi-Component Excitation on the Sliding Response of Unanchored Components in Nuclear Facilities

Aamna Arshad, Dimitrios Konstantinidis, "Effect of Multi-Component Excitation on the Sliding Response of Unanchored Components in Nuclear Facilities", prepared for submission to the Journal of *Earthquake Engineering and Structural Dynamics*

Abstract

During an earthquake, equipment left unanchored in a nuclear facility can slide and interact with safety-critical systems and components, posing a safety risk to the facility. However, computing the response of unanchored components, especially in three dimensions, can be computationally expensive during the preliminary design stages. Nuclear standards acknowledge this by providing an alternate, approximate method for estimating sliding displacement. This paper investigates the effect of bidirectional horizontal interaction and the influence of the vertical component of excitation on the sliding response of unanchored components. It also evaluates the approximate method in ASCE 4-16 and explores multi-component intensity measures for predicting sliding displacement. A cascading analysis approach is taken where a suite of 40 floor acceleration histories obtained from response history analysis of a representative nuclear power plant facility are used

as input to analyze the response of the sliding components. A Bouc-Wen type model is used to determine the nonlinear sliding response of the unanchored components. The computed responses for the sliding components under uni-, bi-, and tridirectional floor excitation are examined, along with the approximate method and it is concluded that the approximate method is significantly overconservative in all cases. The influence of the bidirectional interaction and vertical component of acceleration is greatest for sites with high shaking intensity and at higher friction coefficients. The intensity measures are also dependent on the coefficient of friction; it is found that the most efficient intensity measures, peak floor acceleration and velocity, are not significantly affected by incorporating multiple components of acceleration.

2.1 Introduction

During an earthquake, significant economic losses and disruption are attributed to damage incurred by or caused to the surrounding environment by nonstructural components. For instance, after the 1971 San Fernando Earthquake, the property damage breakdown for a survey of 25 buildings reported that only 3% of the total damage was structural damage, with the rest being attributed to nonstructural components, namely interior finishes [1]. Additionally, during the 1994 Northridge earthquake, the primary costs were associated with the damage caused by nonstructural components, emphasizing that even if there is little-to-no

structural damage, the nonstructural damage can cause hospitals, businesses, and industrial facilities to become inoperable [2].

In nuclear power plants, various components (e.g. cabinets, portable standby generators, electrical transformers) left unanchored due to the need for mobility can interact with safety-critical systems during a seismic event. A report from the International Atomic Energy Agency [3] on the Fukushima disaster following the 2011 Tohoku Earthquake indicates that there were instances of toppling of unanchored equipment within the nuclear power plant facilities. In one instance, a locking device was broken due to the sliding motion of a hatch on rails [3]. Therefore, it is important to be able to adequately predict and design for the movement of unanchored components to reduce the safety risk to the facility.

Shenton [4] identified the five response modes for unanchored rigid objects in two-dimensions: rest, slide, rock, slide-rock, and liftoff (or free flight). The response mode for stockier objects is sliding. The initial response mode is dependent on the width-to-height ratio (B/H) of the object, coefficient of static friction μ_s, and the peak ground acceleration A_g. Typically, the initial mode of response from rest predicts the subsequent behaviour of the block. Shenton categorized the criteria for the initiation of the sliding mode of a rigid block. For low levels of static friction, when $B/H > A_g > \mu_s$, the slide mode governs [4]. In this paper, it is assumed that the height-to-width ratio of each object, in relation to the friction coefficient and base excitation, is conducive to sliding behaviour only. Rock, slide-rock and liftoff modes are beyond the scope of this study.

Estimation of the sliding response under seismic excitation was first considered by Newmark [5], in an effort to estimate the earthquake-induced slippage of dams. Newmark [5] developed a prediction equation for the sliding displacement of a rigid mass subjected to a rectangular acceleration pulse. The sliding displacement of nonstructural components has also been explored by Choi and Tung [6], Kaneko [7], Konstantinidis and Makris [8] [9], Yeow et al. [10], and Konstantinidis and Nikfar [11], among others. A study by Lopez Garcia and Soong [12] concluded that excluding vertical excitation would lead to underestimating sliding displacement, and the extent of this underestimation was highly dependent on the friction coefficient. However, in their study it was assumed that the vertical excitation was equivalent to the horizontal excitation multiplied by a factor. Chaudhuri and Hutchinson [13] investigated the sliding behaviour of laboratory equipment under horizontal unidirectional excitation to develop seismic fragility curves for estimating the vulnerability of small sliding objects. Konstantinidis and Makris [8] also developed fragility curves based on analytical and experimental response of large unanchored laboratory equipment subjected to unidirectional earthquake excitation. More recently, Nikfar and Konstantinidis [14] considered the effect of vertical excitation on the behaviour of sliding objects subjected to unidirectional horizontal excitation with the use of the Stribeck friction model which captures the velocity-dependence of friction.

Bidirectional sliding has not received much attention in the literature. Jangid [15] investigated the seismic response of a structure on a sliding base due to

bidirectional earthquake excitation and determined that the sliding is influenced significantly by the bidirectional interaction of friction forces. In short, the effect of bidirectional and vertical excitation applied to nonstructural components simultaneously has not yet been explored.

Most studies on the seismic response of sliding components have represented the component as a rigid mass resting on a horizontal base moving in one direction. The behaviour of the contract interface between the component and its base has typically been described by Coulomb friction. Although there have been a few studies that considered different static and kinetic friction coefficient values, (e.g. Konstantinidis and Makris [9], and Chaudhuri and Hutchinson [16]) the vast majority have used a common value, μ. Numerically, this type of behavior can be handled using an event-based approach with stick and slip phases, a rate-independent perfectly plastic model with extremely small yield displacement, or a Bouc-Wen hysteretic model [17]. The uniaxial Bouc-Wen hysteresis model is described by a dimensionless hysteretic parameter, z, which obeys the following differential equation:

$$\dot{z} = \frac{1}{U}[\dot{u} - \beta|\dot{u}|\, z\, |z|^{\eta-1} - \gamma\dot{u}|z|^{\eta}] \tag{1}$$

where $\dot{u}$ is the velocity, U is the yield displacement, β and γ are parameters that describe the shape of the hysteresis, and η is the knee sharpness that controls how sharp the transition is from elastic to plastic behaviour [17]. The restoring force is a function of the displacement and hysteretic parameter, z.

The model was expanded upon by Park et al. [18] to include biaxial interaction, in order to model the response of reinforced concrete columns that were significantly affected by biaxial structural interaction in the plastic range. The hysteretic components in both orthogonal directions are determined by solving a pair of coupled differential equations. Wang and Wen [19] generalized the model by Park et al. by extending the governing equation for any value of η. However, this generalization affected the rotational invariance of the model, making it no longer isotropic for values of $\eta > 2$. Harvey and Gavin [20] further extended the Bouc-Wen model making it isotropic for all values of η.

Practically, the modelling of sliding behaviour under multi-component excitation using a Bouc-Wen type model or other approaches can be too complex or computationally expensive for engineers to consider during the initial design stages or routine seismic evaluations. Consequently, the ASCE 43-05 [21] and 4-16 [22] standards allow for the use of an approximate method to determine the peak sliding displacement of unanchored rigid objects. However, the accuracy of this method has not been evaluated in published literature against experimental results or realistic analytical models incorporating multi-component excitation.

With the exception of Konstantinidis and Nikfar [11] [14], who considered the effect of vertical excitation and Jangid [15], who studied bidirectional interaction, the response of an object to multi-component excitation has not been explored in depth, especially with all three components applied simultaneously. This study aims to investigate the influence of bidirectional interaction and the

vertical acceleration on sliding displacement when multi-directional excitation is applied. The paper also compares the accuracy of the approximate method in the ASCE nuclear standards against results from multi-directional sliding models. In addition, it evaluates the SRSS and 100-40-40 spatial combination rules recommended by the ASCE standards for combining independent response components. While intensity measures for sliding displacement have been proposed in [8], [9] and [11], there has not been any investigation into evaluating different intensity measures in relation to sliding displacement. This paper examines twelve intensity measures across a wide range of μ values to determine the most efficient measure. Furthermore, the application of multi-component excitation is extended to intensity measures which are evaluated under bi-, and tri-directional excitation.

2.2 Model Description

Unanchored, stocky nonstructural components, which are prone to sliding, can often be idealized as rigid blocks. The sliding block model considered here consists of a rigid block on a hard surface with a friction coefficient to represent interface roughness. According to Nikfar and Konstantinidis [23], within the range of friction coefficients for sliding equipment, the peak sliding response is mainly influenced by kinetic friction μ_k and not static friction μ_s. Therefore, a simplified Coulomb friction model where $\mu = \mu_k = \mu_s$ is used for the contact interface between the rigid block and floor. Figure 2.2.1 shows a rigid block supported on a rigid base with prescribed acceleration history $\ddot{u}_{fx}$, $\ddot{u}_{fy}$, $\ddot{u}_{fz}$. As mentioned above,

it is assumed that the only response modes are sticking and sliding, and the block does not lose contact with the base. The block will start sliding when $\left(\ddot{u}_{fx}^2 + \ddot{u}_{fy}^2\right)^{0.5} > \mu\left(g + \ddot{u}_{fz}\right)$. The equations of motion for a sliding block subjected to bidirectional excitation are:

$$\ddot{u}_x + \mu_k\left(\ddot{u}_{fz} + g\right)\frac{\dot{u}_x}{\|\dot{\mathbf{u}}\|} = -\ddot{u}_{fx} \tag{2a}$$

$$\ddot{u}_y + \mu_k\left(\ddot{u}_{fz} + g\right)\frac{\dot{u}_y}{\|\dot{\mathbf{u}}\|} = -\ddot{u}_{fy} \tag{2b}$$

where $\dot{u}_x$ and $\dot{u}_y$ are the components of the sliding velocity, $\dot{\mathbf{u}}$, along the x and y directions, g is the acceleration of gravity, and $\|\dot{\mathbf{u}}\| = \sqrt{\dot{u}_x^2 + \dot{u}_y^2}$.

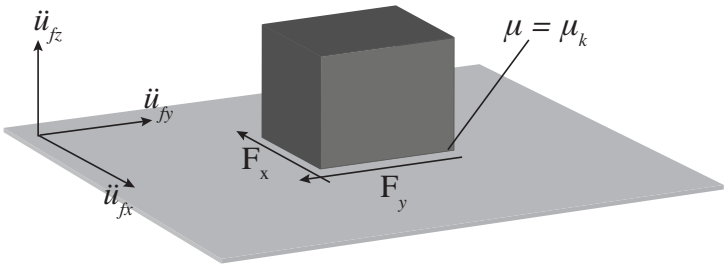

Figure 2.2.1 Unanchored sliding component idealized as a rigid block on a rigid base

This study adopts an isotropic biaxial hysteresis model with arbitrary knee sharpness. The $\dot{u}_x/\|\dot{\mathbf{u}}\|$ and $\dot{u}_y/\|\dot{\mathbf{u}}\|$ terms in Equation 2 are replaced by the hysteretic parameters z_x and z_y, which obey the system of coupled differential equations presented by Harvey and Gavin [20] and referred to herein as the HGBW model:

$$\dot{z}_x = \frac{1}{U_x}\left[A\dot{u}_x - z_x\left(\beta|\dot{u}_x z_x| + \gamma\dot{u}_x z_x + \beta|\dot{u}_y z_y| + \gamma\dot{u}_y z_y\right)\left(z_x^2 + z_y^2\right)^{\frac{\eta-2}{2}}\right] \quad (3a)$$

$$\dot{z}_y = \frac{1}{U_y}\left[A\dot{u}_y - z_y\left(\beta|\dot{u}_x z_x| + \gamma\dot{u}_x z_x + \beta|\dot{u}_y z_y| + \gamma\dot{u}_y z_y\right)\left(z_x^2 + z_y^2\right)^{\frac{\eta-2}{2}}\right] \quad (3b)$$

where U_x and U_y are the yield displacement values in the x and y directions. There is a redundancy with the parameters in the model, which can be eliminated by fixing the value of A as unity [23].

A wide range of friction coefficient values were selected for analysis based on values reported in studies on experimental testing of equipment in medical and other lab facilities. Starting from $\mu = 0.05$ for items on casters [24] to $\mu = 0.8$, which was found to be the upper value for small equipment and contents from a laboratory UC Berkeley [25]. The coupled differential equations are transformed into state-space and solved numerically using MATLAB's ode45 solver. The state vector and its derivative are:

$$\mathbf{y} = \begin{bmatrix} u_x & u_y & \dot{u}_x & \dot{u}_y & z_x & z_y \end{bmatrix}^T \quad (4a)$$

$$\dot{\mathbf{y}} = \begin{bmatrix} y_3 \\ y_4 \\ -\ddot{u}_{fx} - \mu g\left(1 + \frac{\ddot{u}_{fz}}{g}\right)y_5 \\ -\ddot{u}_{fy} - \mu g\left(1 + \frac{\ddot{u}_{fz}}{g}\right)y_6 \\ \frac{1}{U_x}\left[y_3 - y_5\left(\beta|y_3 y_5| + \gamma y_3 y_5 + \beta|y_4 y_6| + \gamma y_4 y_6\right)\left(y_5^2 + y_6^2\right)^{\frac{\eta-2}{2}}\right] \\ \frac{1}{U_y}\left[y_4 - y_6\left(\beta|y_3 y_5| + \gamma y_3 y_5 + \beta|y_4 y_6| + \gamma y_4 y_6\right)\left(y_5^2 + y_6^2\right)^{\frac{\eta-2}{2}}\right] \end{bmatrix} \quad (4b)$$

A very low value for the yield displacement values, i.e. $U_x = U_y = 0.0001$ m is selected to simulate rigid perfectly-plastic behaviour. Sensitivity analysis conducted for parameters η, β, and γ concluded that variation in the parameters did not result in a significant change for the hysteresis, which is attributed to the very small value for yield displacement. Thus, β and γ were taken as 0.5, and 2 was selected for η. It should be noted that the HGBW model is reduced down to the Park-Wen model for η = 2.

2.3 Sliding Model Verification

The HGBW model is first verified for prescribed displacement orbits against the bidirectional Coulomb friction model. Figure 2.3.1 shows the results for a circular orbit (top) and an astroid orbit (bottom). The displacements u_x and u_y are normalized by the amplitude of the prescribed displacement amplitude, u_o , while the forces F_x and F_y are normalized by the frictional strength of the interface, μmg, where m is the mass of the object. For the Coulomb model, $F_x/\mu mg = \dot{u}_x/\|\dot{\mathbf{u}}\|$ and $F_y/\mu mg = \dot{u}_y/\|\dot{\mathbf{u}}\|$ while for the HGBW model, $F_x/\mu mg = z_x$ and $F_y/\mu mg = z_y$. As shown in Figure 2.3.1, the results from the two models nearly overlap.

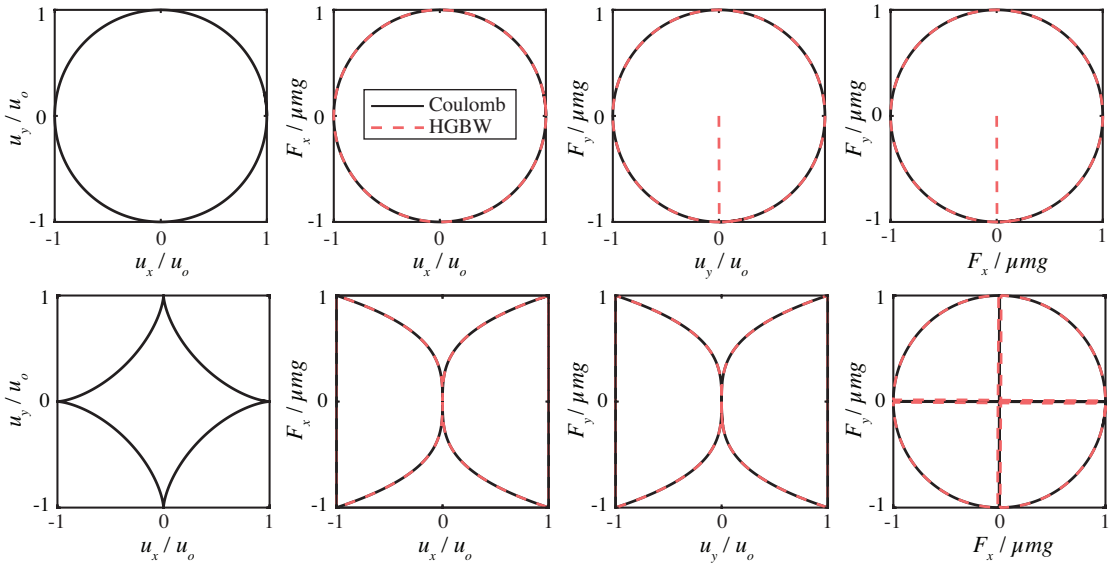

Figure 2.3.1 Comparison of bidirectional Coulomb and HGBW model responses for controlled displacement orbits. Top: circle. Bottom: astroid. (μ = 0.2, u_o = 1 m)

In order to further verify the model, the output from the HGBW model was compared against experimental results. While there are currently no results available in the literature for bidirectional sliding of nonstructural components, experimental tests were conducted by Mokha et al. [27] on Teflon sliding bearings under compression and bidirectional excitation. At the bearing sliding interface, the experimental models showed interaction between the *x* and *y* components of the friction force. A controlled displacement orbit in the shape of a figure-8 was applied to the bearings with the excitation in the *x* and *y* directions as described:

$$u_x = u_{xo} \sin(\omega t) \tag{6a}$$

$$u_y = u_{yo} \sin(2\omega t) \tag{6b}$$

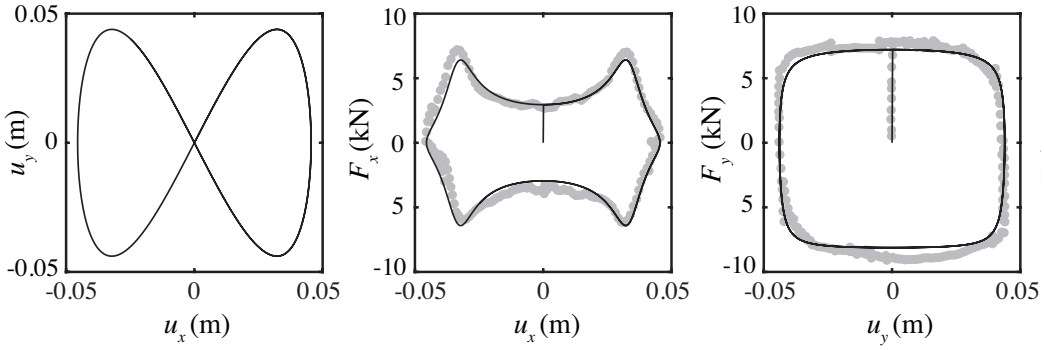

Figure 2.3.2 Comparison of HGBW model (black) with experimental results (gray) from Mokha et. al [27]

where u_{xo} = 45.5 mm, u_{yo} = 43.9 mm and ω = 0.5 rad/s, with a bearing pressure of 3.61 MPa. The coefficient of friction is a function of velocity and other parameters determined to fit experimental data in Mokha et al. [27] Equations (6a, 6b) are used as input for the sliding model and the parameters are calibrated as β = 0.1 and γ = 0.9, the yield displacement U_x and U_y is set as 0.0001 m. The experimental results are reproduced using the HGBW model with good agreement as shown in Figure 2.3.2.

2.4 Analysis Approach

In this study, a decoupled dynamic analysis is followed to investigate the sliding response of unanchored nonstructural components in a nuclear power plant. The horizontal and vertical components of the absolute floor acceleration were used as the excitation components in the equations of motion of the sliding block. The floor acceleration histories were obtained from response history analysis of the

internal structure of a representative nuclear power plant. The internal structure has a total height of 39 m and a mass of 50,000 tons, and was represented by a 3D lumped-mass linear elastic stick model. An original STARDYNE model (courtesy of Ayman Saudy, Kinectrics) was adapted in OpenSees [see Acknowledgements]. The fundamental period of the structure is 0.13 s and 0.14 s in the orthogonal horizontal directions and 0.047 s in the vertical direction. More detailed information about the structural model may be found in Huang et al [28], who used the same internal structure. Linear response history analysis of the stick model was conducted with the suites of ground motions discussed in the next section, with the three ground motion components applied simultaneously. Absolute floor acceleration histories to be subsequently used for the sliding analysis were recorded at an elevation of 18 m.

2.5 Ground Motion Selection and Scaling

Two sites were selected for analysis to cover a wider range of seismic hazard. This is consistent with previous seismic analysis for nuclear power plants where two sites of different seismic intensity are selected for analysis [28], [29]. The two specific locations were selected by overlaying a map of the current operating nuclear power plants in the United States with the 2014 National Seismic Hazard Maps [30]. The majority of nuclear power plants are on the East coast where the seismic hazard is low to moderate with the exception of the Diablo Canyon Power Plant in California, which has the highest seismic hazard. To represent low

to moderate seismic hazard, the Robinson Nuclear Generating Station in South Carolina was selected.

The horizontal target design response spectra were created following the procedure from ASCE 43-05 [21]. Seismic Design Category 5, and Limit State D (essentially elastic behavior) were used, consistent with NRC regulations [31]. The uniform hazard response spectra were obtained from the USGS unified hazard tool using the Conterminous U.S. 2014 v4.1.1 maps [32]. Linear interpolation was used to get the response spectra at a mean annual frequency of exceedance of 1/10,000. Following ASCE 43-05, the uniform hazard response spectra were scaled by a design factor to obtain risk-consistent design response spectra, as shown in Figure 2.5.1 (left).

The vertical target spectra were generated by applying frequency-dependent strike-slip V/H ratios to the horizontal design response spectra. The ratios presented by Gülerce and Abrahamson [33] are applied. The first mode period in the vertical direction is 0.047 seconds resulting in a V/H ratio of 0.65. This is consistent with the general guidelines provided in ASCE 43-05 that impose a 2/3 reduction factor for the entire frequency range for distant earthquakes. The vertical design spectra are shown in Figure 2.5.1 (right).

The 0.2 s period deagraggation for both sites revealed that the main seismic hazard is from near-field earthquakes of magnitude 6-8 for the Diablo Canyon location. For the Robinson site, the main hazard is from distant earthquakes with magnitude 7-8 with some contribution from magnitude 4.5-5.5 earthquakes. The

Diablo site has soil type B according to an analysis of seismic hazard at the power plant by the US Nuclear Regulatory Commission [34]. The soil type at the Robinson location is assumed to be type B, based on a report by the South Carolina Department of Transportation [34] on the area surrounding the plant. The selected ground motions for the Diablo and Robinson sites are listed in Table 2.1 and Table 2.2, respectively.

There is no specific guidance in ASCE 4-16 or ASCE 43-05 on the orientation of the near-field ground motions as applied to the structure. For near-fault sites, such as Diablo Canyon, the FEMA P-1050 [36] standard states that horizontal ground motion components should be rotated and applied in the fault normal and parallel directions to the building [36]. The ground motions obtained from the PEER database were rotated to the fault normal/parallel directions. While this does not always guarantee that the maximum response will be obtained, rotating to fault normal/parallel is recommended over unrotated ground motions [37].

Table 2.1 Selected ground motions for the Diablo Canyon site

#	Earthquake Name	Year	Station Name	Magnitude	Dist. (km)	Vs30 (m/sec)
1	Parkfield	1966	Temblor pre-1969	6.2	16.0	528
2	San Fernando	1971	Castaic - Old Ridge Route	6.6	22.6	450
3	San Fernando	1971	LA - Hollywood Store FF	6.6	22.7	316
4	Tabas Iran	1978	Tabas	7.4	2.1	767
5	Morgan Hill	1984	Coyote Lake Dam - Southwest	6.2	0.5	561
6	Nahanni Canada	1985	Site 1	6.8	9.6	605
7	Loma Prieta	1989	Gilroy - Gavilan Coll.	6.9	10.0	730
8	Loma Prieta	1989	UCSC	6.9	18.5	714
9	Loma Prieta	1989	UCSC Lick Observatory	6.9	18.4	714
10	Northridge-01	1994	LA Dam	6.7	5.9	629
11	Kocaeli Turkey	1999	Gebze	7.5	10.9	792
12	Chi-Chi Taiwan	1999	TCU045	7.6	26.0	705
13	Chi-Chi Taiwan	1999	TCU076	7.6	2.7	615
14	Manjil Iran	1990	Abbar	7.4	12.6	724
15	Tottori Japan	2000	SMN015	6.6	9.1	617
16	Parkfield-02 CA	2004	PARKFIELD - DONNA LEE	6.0	4.9	657
17	Parkfield-02 CA	2004	PARKFIELD - TURKEY FLAT #1	6.0	5.3	907
18	L'Aquila Italy	2009	L'Aquila - V. Aterno -Colle Grilli	6.3	6.8	685
19	L'Aquila Italy	2009	L'Aquila – Parking	6.3	5.4	717
20	Christchurch	2011	LPCC	6.2	6.1	650

Table 2.2 Selected ground motions for the Robinson site

#	Earthquake Name	Year	Station Name	Magnitude	Dist. (km)	Vs30 (m/sec)
21	San Francisco	1957	Golden Gate Park	5.3	11.0	875
22	San Fernando	1971	Cedar Springs Allen Ranch	6.6	89.7	813
23	San Fernando	1971	Tehachapi Pump	6.6	63.8	669
24	Whittier Narrows	1987	Vasquez Rocks Park	6.0	50.4	996
25	Loma Prieta	1989	SF - Rincon Hill	6.9	74.1	873
26	Loma Prieta	1989	So. San Francisco Sierra Pt.	6.9	63.2	1021
27	Landers	1992	Silent Valley - Poppet Flat	7.3	50.9	659
28	Chi-Chi Taiwan	1999	HWA057	7.6	50.6	672
29	Chi-Chi Taiwan	1999	ILA050	7.6	66.9	621
30	Chi-Chi Taiwan	1999	ILA063	7.6	61.1	997
31	Chi-Chi Taiwan	1999	TAP046	7.6	118.3	817
32	Hector Mine	1999	Heart Bar State Park	7.1	61.2	625
33	Tottori Japan	2000	HYGH12	6.6	101.8	677
34	Niigata Japan	2004	FKSH05	6.6	81.0	596
35	Umbria-03 Italy	1984	Gubbio	5.6	15.7	922
36	L'Aquila Italy	2009	L'Aquila – Parking	5.6	11.2	717
37	Iwate Japan	2008	MYG011	6.9	82.9	1424
38	Niigata Japan	2004	SITH05	6.6	118.2	670
39	El Mayor Mexico	2010	Barrett	7.2	85.4	511
40	40204628	2007	Lick Observatory Mt. Hamilton	5.5	13.5	710

The US seismic design maps are based on the maximum direction spectra, which inherently assume that the maximum-direction of ground shaking corresponds with the principal response axes of the structure. While ASCE 43-05 and 4-16 are not specific in their requirements for the type of spectra that should be used in scaling, ASCE 7-16 requires the use of the maximum direction spectra, so these were used for scaling in order to be consistent with the seismic hazard maps.

The frequency range for scaling is referenced in both ASCE 43-05 and 4-16 but not explicitly defined. In ASCE 7-16, the recommended period range for scaling is $0.2T - 2T$ where T is the fundamental period of the structure. The first period for this NPP model in the x and y directions is 0.13s and 0.14s. It was not possible to amplitude-scale the ground motions to fall between 90% - 130% of the target spectrum for the $0.2T - 2T$ range as required by ASCE 43-05 for both ground motion suites. The FEMA P-1050 [35] standard permits for some flexibility on the scaling period range: it is allowed to use a smaller upper bound if the structure does not yield – which is acceptable in this case as the seismic design basis and building model are both limited to 'essentially elastic' behaviour and there is no risk of period elongation due to yielding. The lower-bound requirement is primarily due to higher mode effects, which is less significant because the structural model is very stiff. With this in mind, the authors decided to scale the ground motions to be as close to the target spectrum as possible within a reduced period range of $0.37T - 2T$ for the horizontal Robinson suite. For scaling of vertical excitation, the period ranges were $0.85T - 2T$ and $0.64T - 1.9T$ for the Robinson and Diablo ground motion suites, respectively. The scaled ground motions are plotted in Figure 2.5.1.

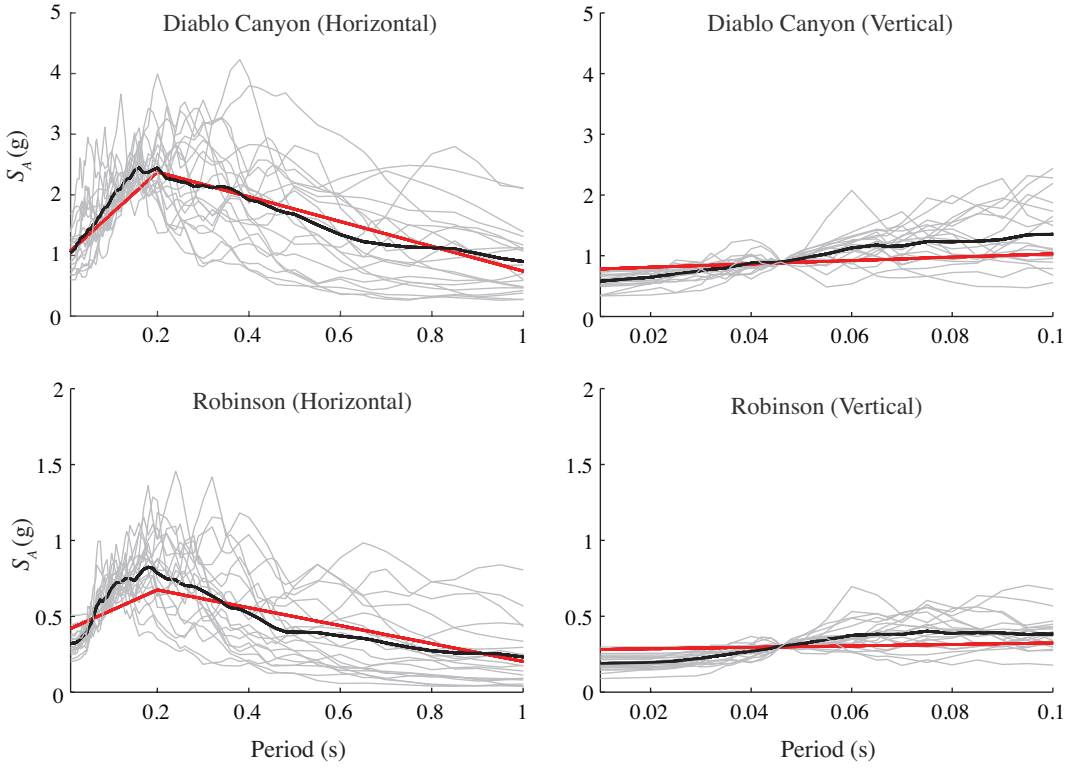

Figure 2.5.1 Target design response spectra (red), scaled ground motions (gray), and mean of the scaled motions (black)

The response history analysis of the NPP model subjected to the Diablo and Robinson site ground motion suite resulted in absolute floor acceleration histories at the floor level of interest. The floor spectra are shown in Figure 2.5.2.

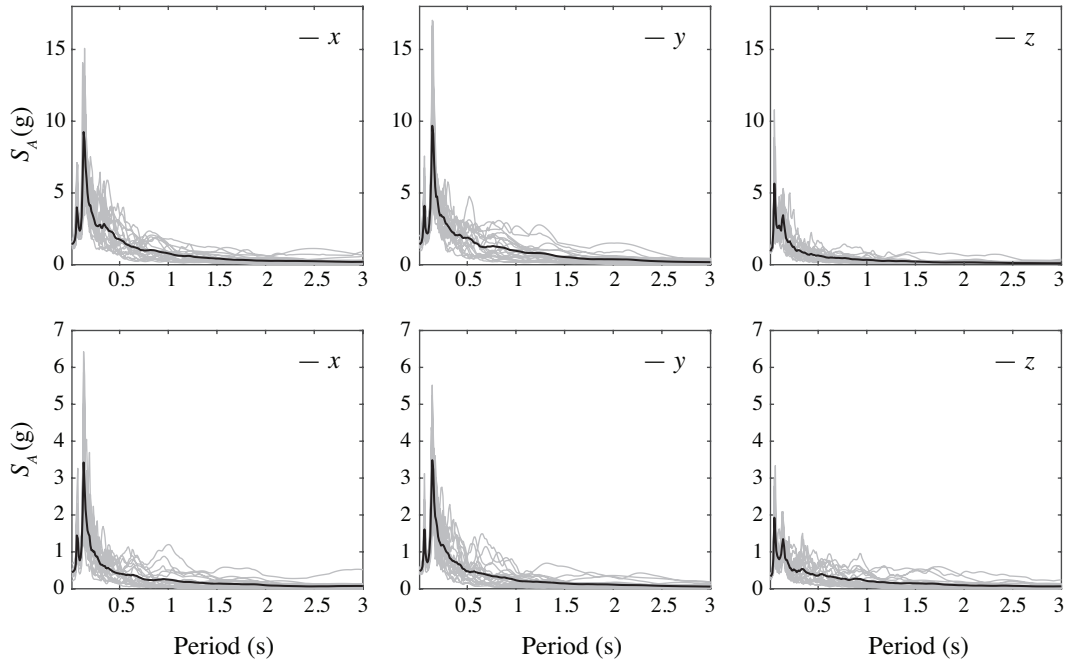

Figure 2.5.2 Floor spectra (2% damping) at the location of the unanchored sliding component in the Diablo (top) and Robinson (bottom) nuclear power plants

2.6 Effect of the Bidirectional Excitation

This section focuses on the effect of bidirectional excitation. Using the floor acceleration histories as input to the HGBW model, the seismic response is analyzed in two ways. Unidirectional (1D) refers to the application of the floor motion in one horizontal directional only, and then independently applied in the second horizontal direction. Bidirectional (2D) refers to the application of the *x* and *y* component of the floor motion simultaneously. The vertical component of the floor acceleration is not applied at this time. Figure 2.6.1 shows the displacement response from the application of three randomly selected floor accelerations. Floor acceleration #1 and #17 from the Diablo location show significantly more

displacement due to higher shaking intensity compared to #26 which is from the Robinson site. The bidirectional orbits also show greater displacement in the *y* direction and *x* directions for #1 and #17, respectively

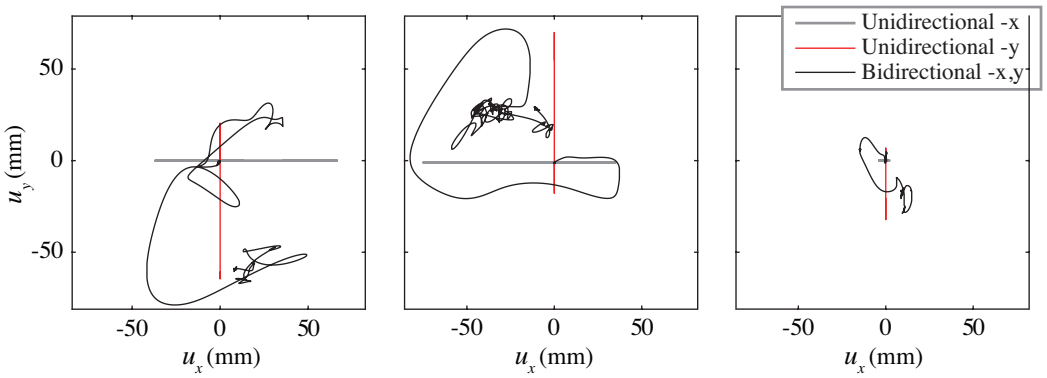

Figure 2.6.1 Sliding displacement orbits in the x-y plane for selected floor motions (#1, 17, 26)

The responses are analyzed in two ways. For each floor motion, the maximum displacement of the component along the *x* and *y* axes are compared individually from the 1D and 2D cases. The responses are also analyzed by calculating the displacement of the component from the origin, which is the maximum of the Euclidean distance: $u \equiv \sqrt{[u_x(t)]^2 + [u_y(t)]^2}$. Figure 2.6.2 plots the average results from this analysis at different values of friction. The '2D' line refers to the application of the *x* and *y*-direction floor acceleration histories simultaneously, whereas '1D' refers to the *x* and *y*-direction horizontal floor motions separately.

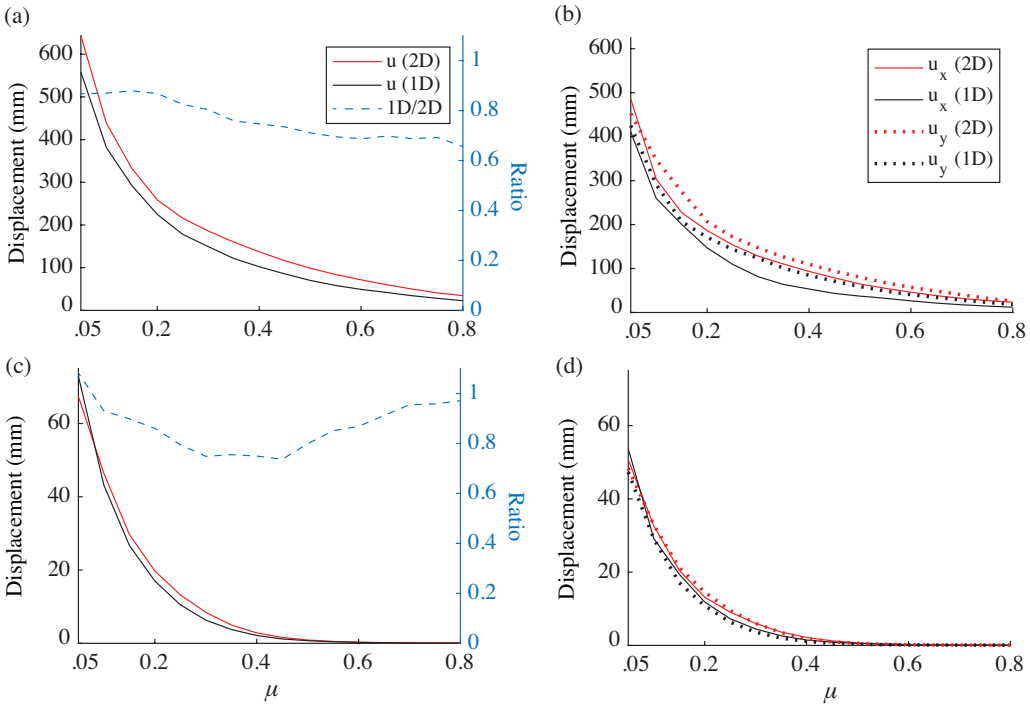

Figure 2.6.2 Effect of the bidirectional excitation on the peak displacement of unanchored sliding components in the Diablo (top) and Robinson (bottom) locations

The effect of the bidirectional interaction is more prominent at the Diablo site which has higher intensity floor motions. The bidirectional excitation results in a higher peak displacement compared to the 1D case in both the *x* and *y* directions. Figure 2.6.2 (top-right) shows a consistent increase in the displacement response by the 2D excitation for all values of friction. When the displacement response is combined, the 1D analysis predicts displacements that are 0.8 times the 2D displacements for $\mu \leq 0.2$, and between 0.65 – 0.8 for $\mu > 0.2$. At the low shaking intensity (Robinson) site the difference between bidirectional excitation and unidirectional excitation is less significant, particularly for low and high friction

coefficient values as shown in Figure 2.6.2 (c). Overall, the observations from the Diablo site agree with those from Jangid's [15] [38] investigation on the response of sliding structures under bidirectional ground motion, where it was also shown that the effects of bidirectional interaction significantly increase the sliding displacement.

2.7 Effect of the Vertical Component of Excitation

In this section, the vertical component of the floor acceleration is applied simultaneously with the horizontal components to determine the effect of the vertical component of excitation on the response of the sliding components. The peak displacement in the *x* and *y* directions as well as the total sliding distance from the origin are plotted in Figure 2.7.1 for the Diablo and Robinson sites. The notation 2D+V refers to the application of the *x*, *y* and *z* components of the excitation simultaneously. Similarly, the 1D+V case denotes the application of the *x* or *y* components of excitation in combination with the vertical (*z*) component. The displacement responses have been averaged across all floor motions.

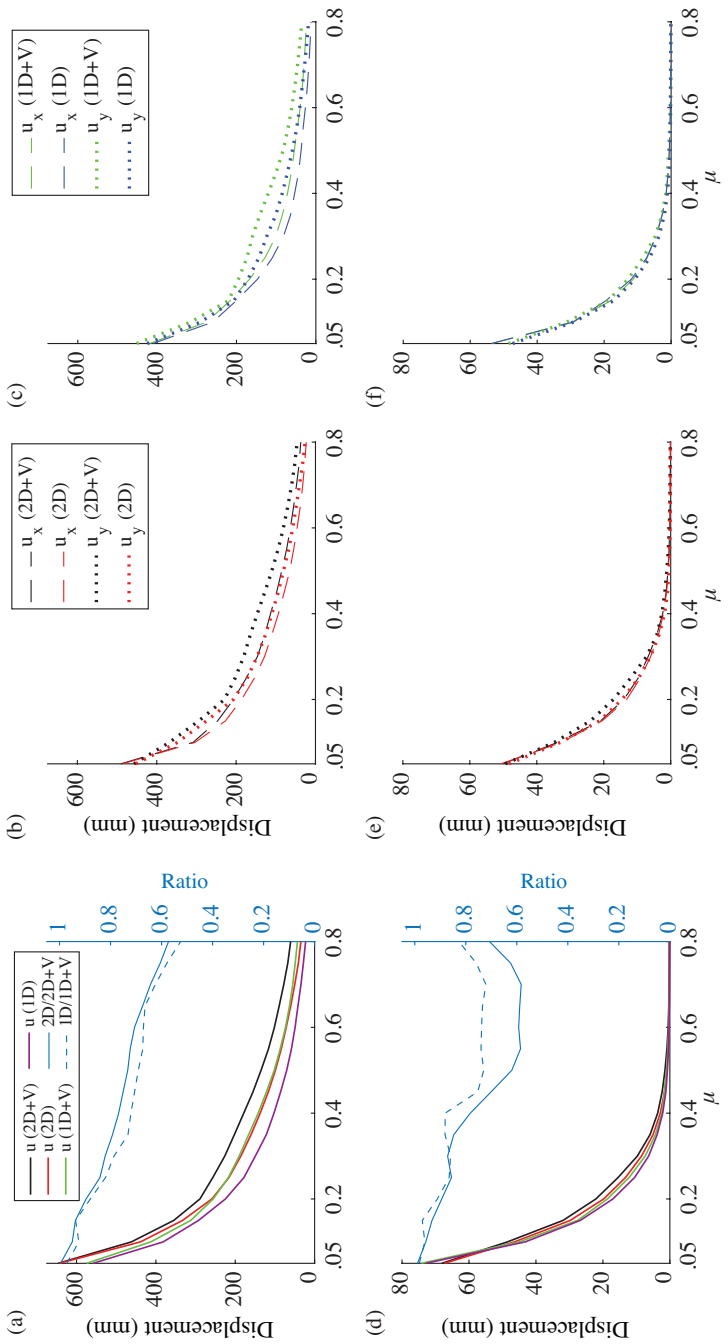

Figure 2.7.1 Effect of the vertical component of excitation on the displacement for Diablo (top) and Robinson (bottom) locations

The application of the vertical components changes the normal force acting on the nonstructural component from mg to $m(g + \ddot{u}_z)$, thereby affecting the frictional force. A vertical acceleration exceeding g would cause the nonstructural component to lose contact with the base; however, none of the floor acceleration histories surpassed g.

At the diablo site (b) and (c) in Figure 2.7.1, it is observed that for $\mu > 0.2$, the vertical excitation significantly increases the sliding displacement along the x and y directions. From the total sliding distance plotted in Figure 2.7.1 (a) and (d), it is clear that at high shaking intensity, the 1D case underestimates the sliding displacement for all ranges of μ.

From Figure 2.7.1 parts (d), (e), (f) it is apparent that at low shaking intensity including the vertical excitation does not alter the sliding displacement response significantly. However, the ratio of sliding displacements between the 1D and 1D+V analysis and from the 2D to 2D+V analysis cases remain similar for both sites. Estimates for sliding displacement from the 1D and 2D cases start at 0.95 times the displacements given by the 1D+V and 2D+V analysis and decrease linearly to 0.7 at $\mu = 0.4$. Beyond $\mu = 0.4$, at the Robinson site, the effect of the vertical excitation is larger in the presence of bidirectional interaction. However, it should be noted that the ratios are less meaningful since the magnitude of the displacements is too low (less than 1mm) to be considered significant. The ground motions which are scaled to a lower seismic hazard have a lower intensity and do not induce sufficient movement of the components at the floor level when the

friction coefficient is higher. For this reason, it is considered acceptable to use the simpler 2D and 1D analysis cases for $\mu > 0.4$ at low seismic intensity site, Robinson.

The observations agree with the study conducted by Lopez Garcia and Soong [12] where it was found that vertical base excitation contributes significantly to the displacement of nonstructural components, particularly for higher values of the coefficient of friction. The study developed vertical excitation histories by multiplying the horizontal excitation by a factor, k. Investigation of sliding displacements under vertical excitation by Konstantinidis and Nikfar [11] found the opposite, where it was concluded that the vertical excitation did not contribute significantly to sliding displacement. This discrepancy may be due to the differences in the structures examined. While this paper and the study by Lopez Garcia and Soong uses the response from fixed-based structures, the result from Konstantinidis and Nikfar is from base-isolated buildings.

Overall the bidirectional interaction and vertical component of acceleration have a significant impact on the peak sliding displacement in some cases. This is especially evident for the Diablo site which has higher shaking intensity, and the effect is more pronounced for larger values of μ. Practically, it is not advisable to estimate sliding displacement from unidirectional excitation at sites with high seismicity.

2.8 Evaluation of the ASCE 43-05 and 4-16 Approximate Method for Sliding

The ASCE 43-05 [21] and 4-16 [22] standards include the same approximate method for estimating peak sliding displacement which is acceptable to use for a symmetric unanchored rigid body. The standards consider a range of friction coefficient values from 0.3-0.7 to be reasonable for the sliding of a rigid object on concrete or steel. This section will focus on comparing the total displacement response obtained using the approximate method against the results from the HGBW model in order to evaluate the accuracy of the ASCE approximate method.

The approximate method detailed in the standard specifies an *effective* friction coefficient, μ_e computed from:

$$\mu_e = \mu\left(1 - 0.4\frac{A_v}{g}\right) \tag{7}$$

where A_v is the peak vertical acceleration and g is the acceleration due to gravity. While the standard does not explicitly state the origin for this equation, a similar equation was proposed by Taniguchi and Miwa [39], where the coefficient of friction was reduced by a factor related to the standard deviation of the ratio of the vertical ground acceleration to the peak vertical ground acceleration at the time of peak horizontal shaking. The equation was originally proposed to provide a safety margin for estimating the sliding displacement for a given base motion without considering the vertical acceleration history. Taniguchi and Miwa assumed a uniform reduction in the friction coefficient (that would result in increased

displacement) when vertical earthquake accelerations were present. The ASCE standard assumes that this ratio is 0.4.

The validity of this estimate is investigated by comparing the displacement, u, of the unanchored object when subjected to all three floor motion components applied simultaneously against the assumption of using an effective friction coefficient in place of applying the vertical acceleration. The results are plotted in Figure 2.8.1.

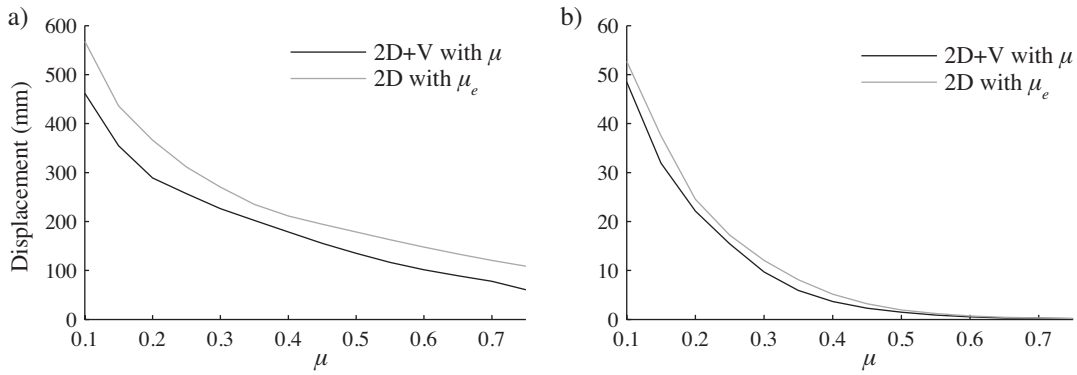

Figure 2.8.1 Sliding spectra comparison of effective friction coefficient against the 2D+V results for a) Diablo and b) Robinson sites

As shown from the comparison in Figure 2.8.1, the effective friction coefficient is excessively conservative for the Diablo and Robinson ground motion sets. The displacement estimates using the effective friction coefficient range from 1.1 to 1.5 times the displacement results from the 2D+V analysis: with estimates becoming more overconservative as the friction coefficient increases. The ASCE standard acknowledges that reducing the friction coefficient by $0.4A_v/g$ is probably very conservative but does not offer any other options at this time.

The approximate method is based on approximating the hysteretic nonlinear sliding behaviour by an equivalent linear system. The method proceeds by defining a *sliding coefficient* as:

$$c_s = 2\mu_e g \tag{8}$$

The next step is to determine the lowest natural frequency, f_{eS} at which the horizontal 10% damped vector spectral acceleration is equal to the sliding coefficient. 10% damping is based on equating the hysteretic energy dissipated by sliding to the energy dissipated by viscous damping in an equivalent linear system. This results in 32% damping, which is reduced to 10% based on data from response history analysis tests [22]. The 10% damped vector spectral acceleration is calculated from:

$$SA_{VH} = [SA_{H1}^2 + 0.16SA_{H2}^2]^{1/2} \tag{9}$$

where SA_{H1} and SA_{H2} are the 10% damped spectral acceleration for the horizontal components, and $SA_{H1} > SA_{H2}$. Then, the best estimate for the sliding distance is determined using:

$$\delta_s = \frac{c_s}{(2\pi f_{eS})^2} \tag{10}$$

The results from using the approximate method are compared against the 2D+V model results and plotted in Figure 2.8.2.

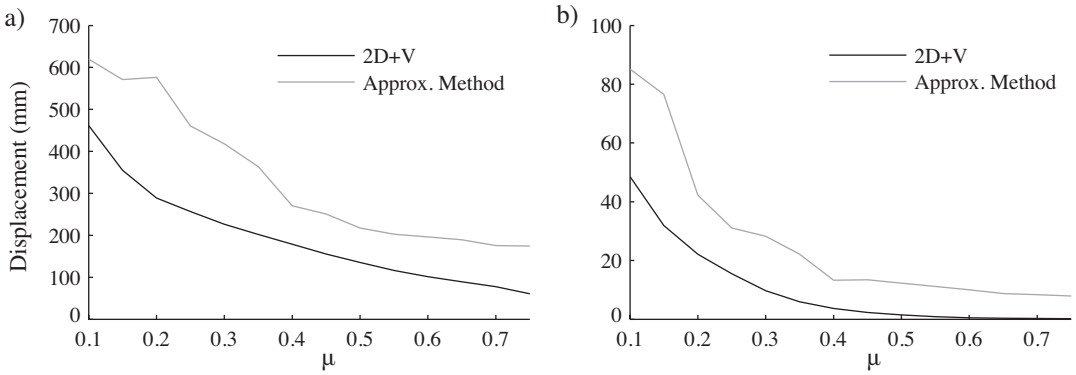

Figure 2.8.2 Sliding spectra comparison of ASCE Approximate Method with the HGBW model for a) Diablo and b) Robinson sites

In both cases, the approximate method significantly overestimates the sliding displacement, particularly for lower friction coefficient values and more so for higher shaking intensity. At high shaking intensity, the approximate method consistently overestimates the displacement by a factor of approximately 1.5 to 1.9 until $\mu = 0.6$, and up to 2.9 for higher friction coefficient values. This may be attributed to the effective friction coefficient which is greatly reduced due to the vertical excitation. For sites with low shaking intensity, the approximate method is especially inaccurate at high friction coefficients, overestimating the displacement response by a factor of up to 45 for $\mu > 0.5$. The ASCE 43-05 standard prescribes a safety factor of 3 for any nonlinear sliding analysis and a safety factor of 2 for the approximate method, to acknowledge its conservativeness. When these factors are applied, the overconservativeness of the approximate method in comparison to the

2D+V model is reduced, but not eliminated. However, the ASCE 4-16 standard prescribes a safety factor of 1.5 for both methods which does not compensate for the overconservativeness of the approximate method.

2.9 Spatial Combination Rules

The ASCE 4-16 and 43-05 standards also allow for combining component responses for each axis of excitation. The standards allow for the use of either the square-root of the sum of the squares (SRSS) method and the 100-40-40 rule. The spatial SRSS rule is described by:

$$R = \sqrt{R_x^2 + R_y^2 + R_z^2} \tag{11}$$

where R_x, R_y, R_z are the maximum responses of the object in the three orthogonal directions due to application of the corresponding components of floor excitation. In this case, since the object is sliding on the *x*-*y* plane, the response is limited to R_x and R_y only. From a time history analysis perspective, these responses do not necessarily occur at the same time step. While these methods are typically meant to be used for response spectrum analyses, past standards (namely ASCE 4-98 and NRC RG 1.92) allow for the use of the 100-40-40 rules and SRSS method for the time history method [40].

For comparing the displacement response, the process can be generalized as taking the maximum displacements in the *x* and *y* directions and combining those responses using either $R_x + 0.4R_y$ or $0.4R_x + R_y$, whichever yields the

maximum result. The rule was first proposed by Newmark and Hall [40] as a conservative alternative to the SRSS method for the design of nuclear power plants.

Both of these spatial combination rules are compared against the 'exact solution,' considered here to be the maximum of $u \equiv \sqrt{[u_x(t)]^2 + [u_y(t)]^2}$ from the 2D+V analysis. The maximum value from all the time steps is retained and averaged over the suite of 20 floor motions. Figure 2.9.1 plots the comparison of the SRSS and 100-40-40 spatial combination rules along with the exact displacement.

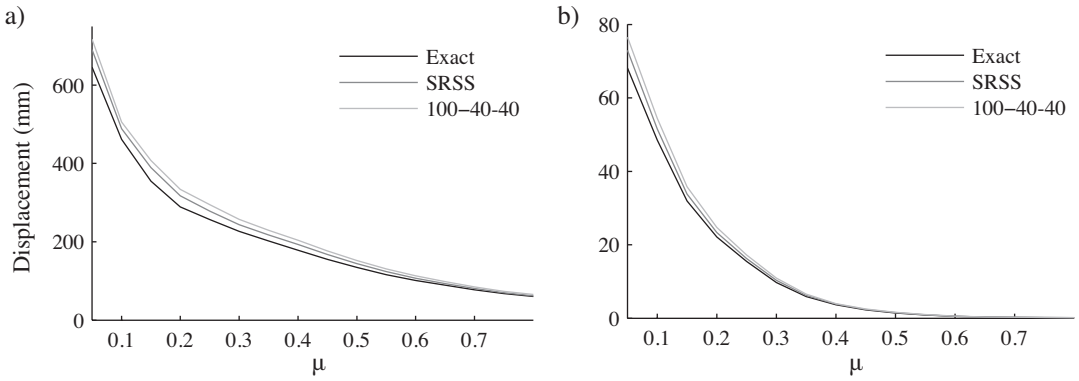

Figure 2.9.1 Comparison of sliding spectra for the exact (2D+V), SRSS, and 100-40-40 spatial combination rules for a) Diablo and b) Robinson site

Note that the 100-40-40 rule is slightly more conservative than the SRSS method. The difference is more pronounced for lower friction coefficients, and generally for higher shaking intensity. This result agrees with Nie et. al [40] where it was found that the 100-40-40 rule is almost always more conservative compared to the SRSS method.

2.10 Intensity Measures

This study aims to identify good intensity measures (IMs) for better predicting the displacement of sliding objects in nuclear power plants. In performance-based earthquake engineering, an intensity measure (IM) is a parameter that characterizes earthquake shaking. Unlike structural demand parameters, which are linked to IMs related to the ground motion, demands on nonstructural components are linked to the response of the structure. Therefore, in this context of sliding components resting on the floor, the IMs were evaluated based on floor excitation.

The demand parameter of interest in this investigation is the peak sliding displacement, U_{max} which varies according to the coefficient of friction for each floor motion.

Since the datasets only contain positive values it is commonly assumed that the U_{max} is lognormally distributed [8], [9]. Another typical assumption is that the relationship between the mean of U_{max} and the IM is described by the scale law: $U_{max} = a(IM)^b$, which can be transformed into the equation of a straight line in the log-log plane [42], [43]:

$$\ln(U_{max}) = \ln(a) + b \ln(IM) \tag{12}$$

where a and b are regression coefficients describing the y-intercept and slope of the line which best fits the data.

Regression analysis is conducted to determine the correlation between the U_{max} and various IMs. The coefficient of determination R^2, is used to calculate the

goodness of fit and estimate how closely the data can be approximated by the linear model. An adjusted R^2 [44] value is calculated for each regression. This accounts for the bias in the number of variables used to fit a regression model. While it is not a large adjustment for a linear model with 2 regression coefficients, an adjusted R^2 value is typically lower than an ordinary R^2 value. Henceforth, reference to R^2 from this point on will be referring to the adjusted R^2 value. The IMs are evaluated primarily on their efficiency which is judged based on the R^2 value. Since U_{max} varies with μ, R^2 is also dependent on friction.

A variety of IMs were selected for evaluation. The simplest of which include peak floor acceleration (PFA), peak floor velocity (PFV) and peak floor displacement (PFD). The definitions for the following IMs are based on the study of rocking amplification and strong motion duration by Giouvanidis and Dimitrakopoulos [45] but adapted for sliding motion instead of rocking. The IMs include uniform duration, t_{uni}, which is the total duration of time that the horizontal acceleration history exceeds the minimum threshold to initiate sliding, which is μg for the 1D case. The bracketed duration, t_{brc}, is calculated as the time difference between the first and last time that the floor acceleration exceeds the minimum threshold for sliding. The cumulative absolute velocity (CAV) was first introduced with a minimum threshold value above which the acceleration history would be counted to reduce the influence of (low intensity) ground motion duration from introducing bias to the results [46]. The CAV has been used with a modified threshold value in other cases when evaluated as an IM for liquefaction and rocking

behaviour [47][45]. The present study defines CAV_{exc} is as the time integral of the acceleration history for the period in which it exceeds a threshold, which will be set as the minimum sliding threshold, μg.

For IMs such as t_{uni}, t_{brc} and $CAV_{exc,}$ where the threshold is defined as μg, the analysis was conducted for all friction coefficients ranging from 0.05 to 0.8. The average duration of the IM across all friction coefficients was used for each ground motion.

Other IMs include Arias Intensity, I_A, which is a measure of the total energy per unit weight for the total duration of earthquake shaking [48]. The root mean square acceleration, A_{RMS}, is the sum of the energy at all frequencies divided by the total duration, thus it represents the average rate of energy from the earthquake. The Fajfar index, I_F, combines PFV with the significant duration t_{sig} and was introduced by Fajfar et. al [49] as a way to measure the damage capacity of ground motions. The significant duration, t_{sig}, is the interval of time between 5% and 95% of Arias Intensity for the earthquake acceleration history. The characteristic intensity, I_C, was proposed by Park et. al [50] and is calculated as a combination of A_{RMS} and t_{sig}.

Lastly, an IM based on the spectral ground acceleration proposed by Nikfar and Konstantindis [11] as a dimensionless IM for sliding equipment in base-isolated buildings is also evaluated. The dimensionless IM factors into account the spectral ground acceleration and the friction coefficient. The period chosen for the IM in order to determine the spectral acceleration was 0.14s which is the first-mode period for the structure and damping was assumed to be 5%. All the evaluated IMs

are summarized in Table 2.3. The input for analyzing one-component IMs was the horizontal excitation in the *x* direction.

Table 2.3 Summary of selected intensity measures

IM	Name	Calculation
1	Peak Floor Acceleration	$PFA = \max(\lvert \ddot{u}_f(t) \rvert)$
2	Peak Floor Velocity	$PFV = \max(\lvert \ddot{u}_f(t) \rvert)$
3	Peak Floor Displacement	$PFD = \max(\lvert u_f(t) \rvert)$
4	Uniform Duration	$t_{uni} = \sum_{dt=0}^{t/npts} \langle x \rangle \, dt$, where $\langle x \rangle = \begin{cases} 0 \; for \; \lvert \ddot{u}_f(t) \rvert < \mu g \\ 1 \; for \; \lvert \ddot{u}_f \rvert (t) \geq \mu g \end{cases}$
5	Bracketed Duration	$t_{brc} = \max(t_{uni}) - \min(t_{uni})$
6	Cumulative Absolute Velocity of Exceedance	$CAV_{exc} = \int_0^t \langle x \rangle \, \ddot{u}_f(t) \, dt$, where $\langle x \rangle = \begin{cases} 0 \; for \; \lvert \ddot{u}_f(t) \rvert < \mu g \\ 1 \; for \; \lvert \ddot{u}_f(t) \rvert \geq \mu g \end{cases}$
7	Significant Duration	$t_{sig} = t_{95\% \, I_A} - t_{5\% \, I_A}$
8	Arias Intensity	$I_A = \frac{\pi}{2g} \int_0^t \ddot{u}_f(t)^2 \, dt$
9	Root Mean Square Acceleration	$A_{RMS} = \sqrt{\frac{1}{t} \int_0^t \ddot{u}_f(t)^2 \, dt}$
10	Fajfar Index	$I_F = PFV \cdot (t_{sig})^{0.25}$
11	Characteristic Intensity	$I_c = {A_{RMS}}^{1.5} {t_{sig}}^{0.5}$
12	Normalized Excitation Strength	$IM_{12} = \frac{SA(T,\zeta)}{\mu g}$ -1

For brevity, the comparison of IMs against the 1D, 2D and 1D+V models is not shown here. The IMs are compared against the most realistic displacements which are obtained from the 2D+V sliding model. These displacements vary based on which friction coefficient was used in the analysis. Figure 2.10.1 and Figure

2.10.2 show the regression analysis for all IMs at specific friction coefficients of 0.15 and 0.55, respectively.

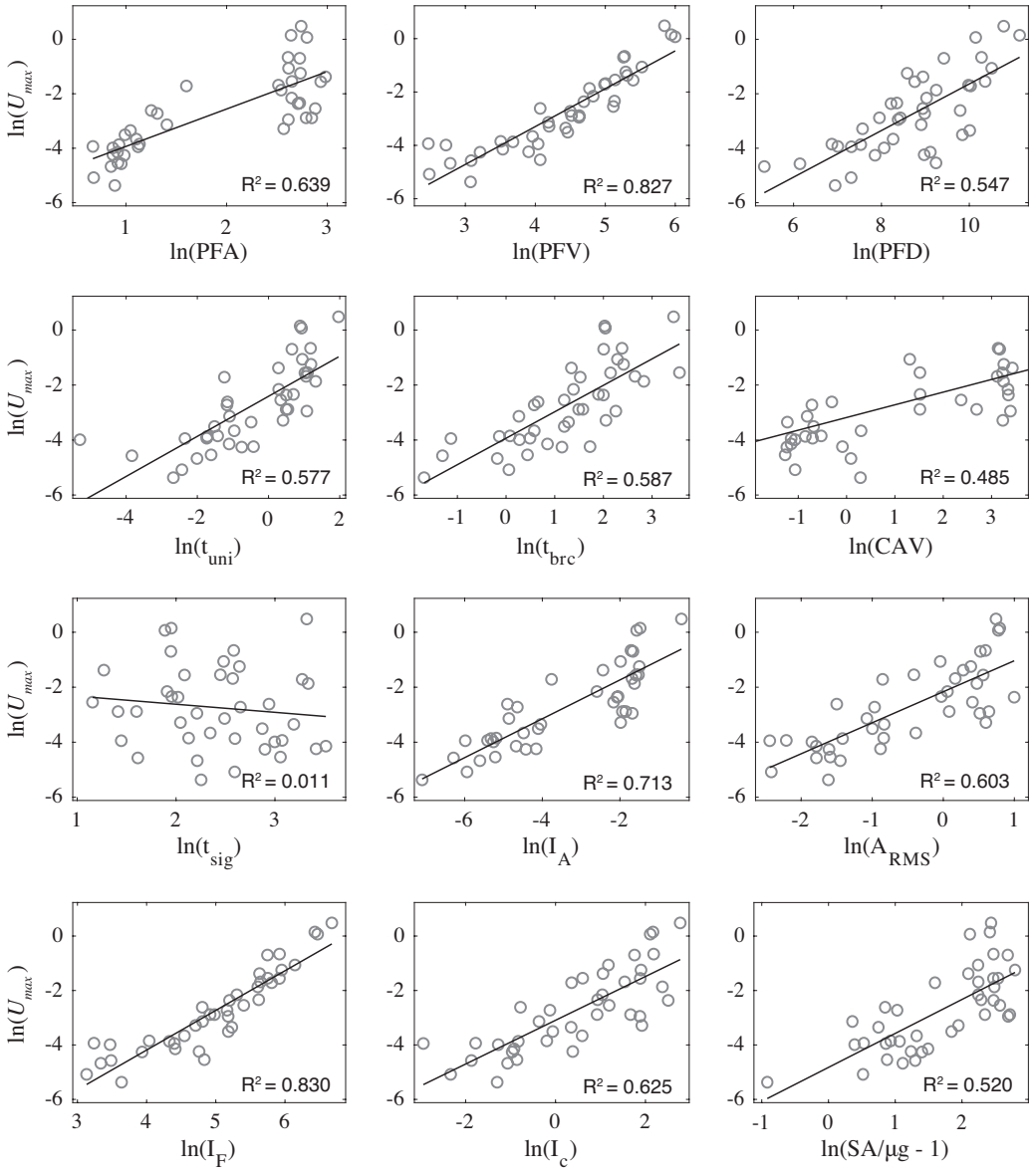

Figure 2.10.1 Regression analysis of peak displacement (at μ = 0.15) for one-component intensity measures

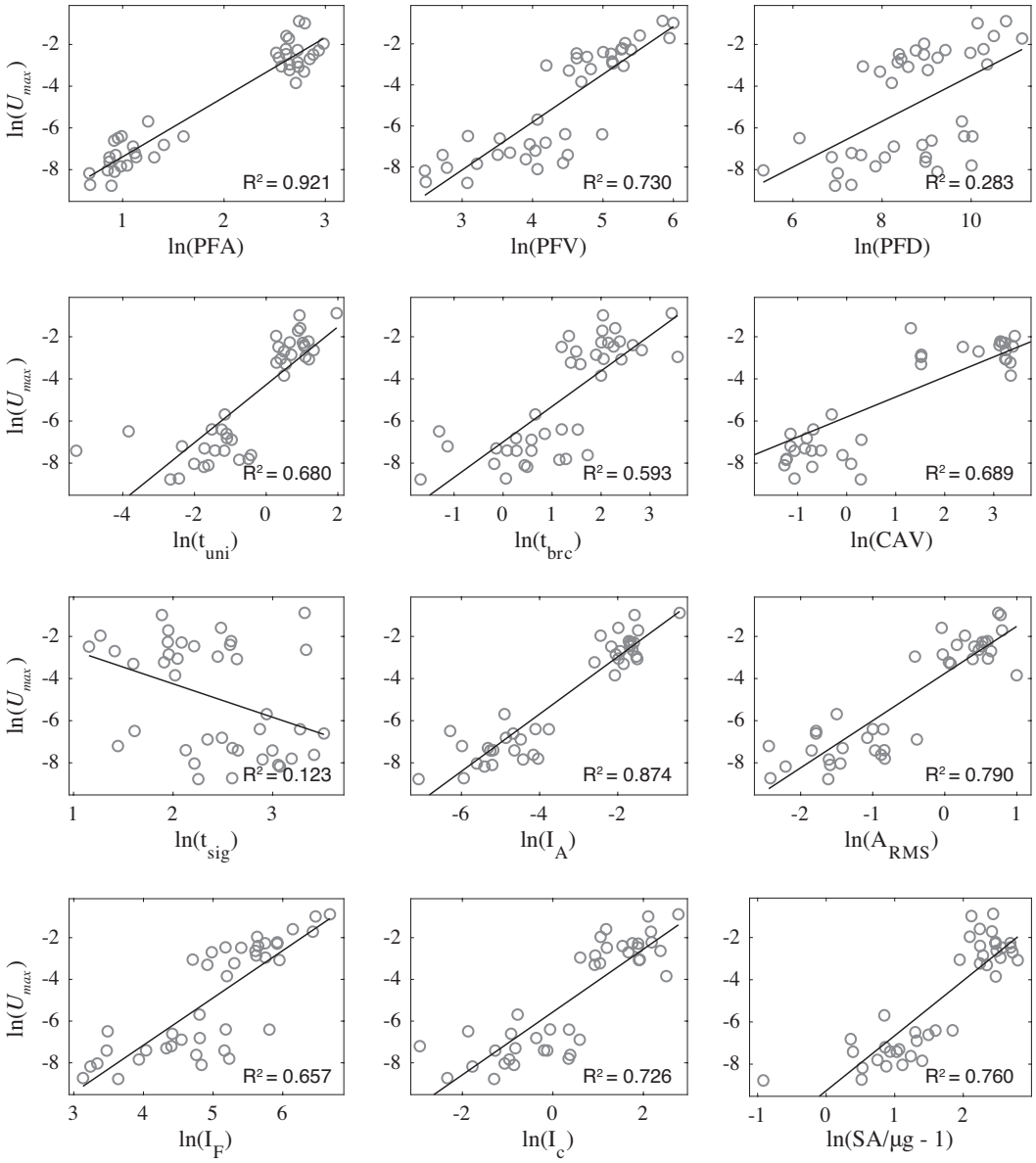

Figure 2.10.2 Regression analysis of peak displacement (at μ = 0.55) for one-component intensity measures

For a lower friction coefficient (μ = 0.15), the most efficient IM is PFV, followed by I_F which is a combination of the floor velocity and duration of the ground motion. Figure 2.10.1 also reveals that IMs which factor acceleration into their calculations show a significant grouping of the data at the low and high displacement ranges. This is due to the nature of the 40 ground motions selected: 20 ground motions are scaled based on high ground acceleration intensity and 20 are applicable to low ground acceleration intensity. This clustering phenomenon due to ground acceleration intensity was also observed by Giouvanidis and Dimitrakopoulos [44] for the evaluation of rocking intensity measures. This grouping is less apparent for IMs which incorporate velocity into their calculation.

At a higher friction coefficient (μ = 0.55), Figure 2.10.2 also shows this grouping of data, and the clustering becomes tighter for IMs such as PFA and I_A, which results in a better goodness of fit for the regression line. The significant duration, t_{sig}, showed a negative correlation indicating that floor motions where the intensity is concentrated over a shorter duration result in more sliding displacement. It should also be noted that results for higher friction coefficients may be biased due to the lack of displacement at higher friction for ground motions at the Robinson site. It is also apparent that the best intensity measure at a higher friction coefficient is PFA, closely followed by I_A.

When the ground motion sets for the two sites are separated for the regression analysis, the relative correlations observed for velocity-based IMs at μ = 0.15 and μ = 0.55 still hold true, albeit with lower R^2 values. For instance, at μ =

0.55, R^2 related to PFV is reduced from 0.730 to 0.533 at the Robinson site. A summary of the results from separating the analysis is given in Table 2.4. PFA and other intensity measures which utilize acceleration in their calculations are significantly affected by separating the analysis. This is likely due to the close correlation between larger sliding displacements observed from the Diablo ground motion set, which were scaled based on spectral acceleration. When the analysis is separated there is less variation in the data for acceleration-based IMs resulting in lower correlations.

Table 2.4 Comparison of R^2 for IMs at Diablo and Robinson Sites

IM	R^2 All	R^2 Diablo	R^2 Robinson	R^2 All	R^2 Diablo	R^2 Robinson
		$\mu = 0.15$			$\mu = 0.55$	
PFA	0.639	0.055	0.676	0.921	0.035	0.341
PFV	0.827	0.840	0.533	0.730	0.621	0.262
I_A	0.713	0.311	0.451	0.874	0.228	0.149
I_F	0.830	0.896	0.556	0.657	0.602	0.237
A_{RMS}	0.603	0.001	0.206	0.790	0.002	0.056
IM_{12}	0.625	0.055	0.073	0.760	0.020	0.286

The coefficient of determination, R^2 is calculated for all intensity measures at each friction coefficient. Figure 2.10.3 plots the R^2 value across all μ for the top six IMs. When considering just one-component (1D) IMs, it becomes apparent that the IMs are not consistently efficient across the entire range of friction. For $\mu < 0.3$ IMs which are primarily velocity-based such as PFV and I_F have the highest coefficient

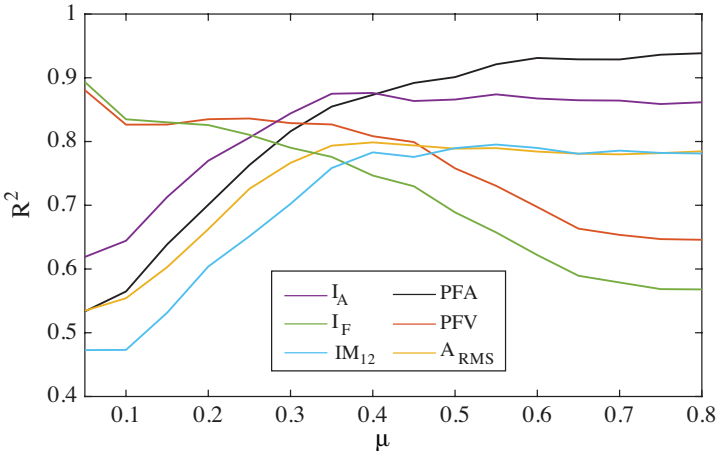

Figure 2.10.3 Comparison of one-component IM efficiency with respect to the coefficient of friction

of determination. At mid to high friction coefficients ($\mu > 0.3$), IMs which include acceleration in their calculations, such as PFA and I_A are the most efficient.

2.11 Intensity Measures for Multi-Component Excitation

Typically, analysis of IMs includes only one component of the input motion. Of interest here is to determine if the IMs can be more efficient by including the orthogonal horizontal acceleration component in the definitions of the IMs. The 12 IMs from Table 2.3 were adjusted to include both horizontal components of the floor motion. The input for the IMs was modified from just the horizontal x

component to $p(\mathrm{t}) = \left([\mathrm{p}_x(t)]^2 + [\mathrm{p}_y(t)]^2\right)^{1/2}$, where p is the floor excitation (i.e. displacement, velocity, or acceleration). For IM_{12}, the input was changed to $\left([\mathrm{SA}_x]^2 + [\mathrm{SA}_y]^2\right)^{1/2}$ to incorporate the x and y floor excitation. IMs which incorporate both horizontal components are referred to as '2D' in this discussion.

The vertical component of acceleration was also incorporated into the intensity measures to see if their efficiency could be further improved. The vertical component of acceleration was included into the intensity measures in three different ways, depending on the type of the IM. For PFA, PFV and PFD the vertical component was incorporated by taking the Euclidean norm of the excitation vector with all three components: $p(\mathrm{t}) = \left([\mathrm{p}_x(t)]^2 + [\mathrm{p}_y(t)]^2 + [\mathrm{p}_z(t)]^2\right)^{1/2}$. IMs which incorporate all three components are referred to as '3D'.

Similarly, for intensity measures such as A_{RMS} the term within the integral is changed to the norm of the 3-component acceleration vector. Interestingly, Arias [47] intended for I_A to be calculated for each orthogonal component of horizontal acceleration and for the total intensity to be represented as the sum of I_A for the x and y directions, since I_A is a scalar measure of intensity [51]. In recent literature, most calculations of I_A are based on a single component of ground motion acceleration [42], [47], [52]. Thus, to include all components of the acceleration vector, Arias intensity was calculated as $I_{A,x} + I_{A,y} + I_{A,z}$.

To include vertical acceleration for certain intensity measures with a threshold, the threshold value was modified from μg to $\mu(g + \ddot{u}_{gz})$, where $\ddot{u}_{gz}$ is

the instantaneous vertical floor acceleration. For the dimensionless $IM_{12,}$ the vertical component was incorporated by replacing μ with the effective friction coefficient, μ_e as defined by ASCE 4-16 and 43-05. Recall that μ_e is used in the approximate method to simulate the influence of the vertical component of acceleration. Figure 2.11.1 plots the R^2 value for all friction coefficients for 1, 2, and 3-componenet IMs.

While most of the intensity measures were improved slightly with the addition of the second horizontal component, IMs that showed significant improvement in efficiency were: PFD, t_{uni}, CAV_{exc}, and IM_{12}. The efficiency of the IMs did not improve substantially when the vertical component of acceleration was also factored into the calculations. This was regardless of how it was implemented either as the threshold value $\mu(g + \ddot{u}_{gz})$, as the Euclidean norm of the 3-component excitation vector, or as μ_e. Since the maximum sliding response, U_{max} occurs on the *x-y* plane it might be why the vertical excitation did not increase the correlation between the IMs and U_{max}.

Interestingly, PFA, PFV, t_{brc}, I_F, A_{RMS} did not show a significant difference between 1D, 2D, and 3D cases. Additionally, IMs such as t_{uni} and t_{brc} maintain their efficiency for all values of friction. It is recommended that for $\mu < 0.3$, PFV and I_F should be used, for $\mu > 0.3$, PFA and I_A are the most efficient for 1D excitation. When considering 2D excitation, IM_{12} becomes a good choice for $\mu > 0.55$.

The top IMs such as PFA, PFV, I_F, are largely unaffected by introducing multiple components. I_A does benefit slightly with the addition of the second horizontal component but still performs well under 1D excitation.

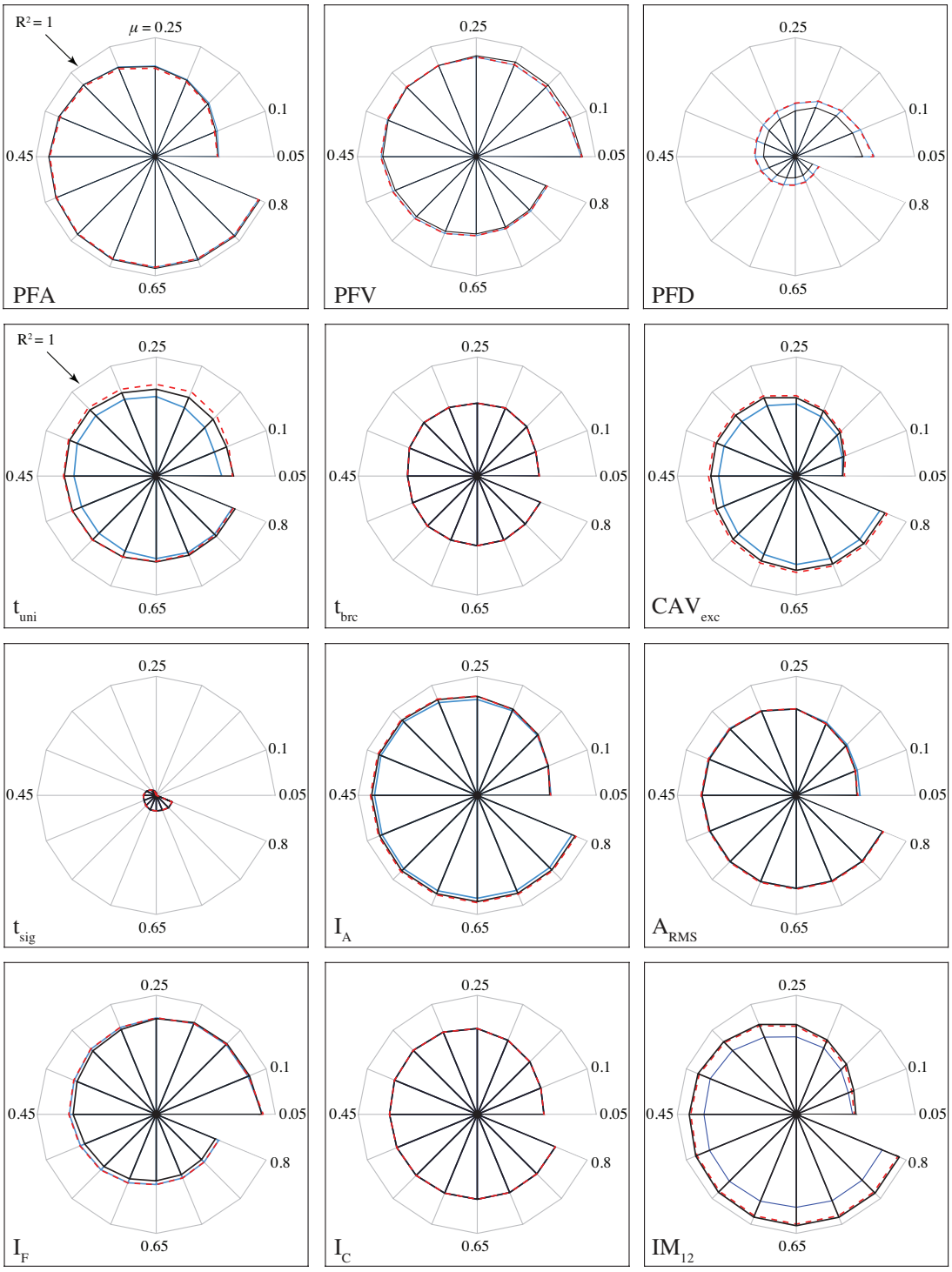

Figure 2.11.1 Efficiency of intensity measures for multi-component excitation: 1D (blue), 2D (red), and 3D (black) with respect to the friction coefficient

2.12 Conclusions

This study investigated the seismic response of rigid nonstructural components within a NPP. The displacement response was analyzed under multicomponent 1D, 1D+V, 2D, and 2D+V excitation. From this analysis, the effect of bidirectional interaction and vertical component of excitation is summarized below. Recommendations are given based on two potential sites with high and low shaking intensities. Evaluation of the ASCE approximate method and its spatial combination rules are also summarized. The concept of multi-component excitation is expanded to IMs. A variety of IMs were investigated to determine the best IM for predicting sliding displacement.

At the lower seismic intensity site (Robinson) and for $\mu > 0.4$ it is acceptable to use any model, as they all converge to a very low displacement for higher friction coefficients. For $\mu \leq 0.4$ the 1D analysis case can predict displacements that are approximately 0.7 times the displacements from the 2D+V analysis. Overall, for low seismic hazard sites such as the Robinson nuclear power plant, the influence of the vertical component of acceleration and bidirectional interaction is less of a concern.

At the high seismic intensity site (Diablo), it is not advisable to use the 1D model since, at best, it underestimates the response by a ratio of 0.87 for low friction coefficients; and up to 0.66 for high friction. The ratios can translate to significant differences in the sliding displacement since the high shaking intensity of the site leads to a larger displacement response. The differences between the four analysis

cases are also more pronounced for the Diablo Canyon nuclear power plant site due, in part, to larger sliding displacements from higher-intensity floor motions. It is found that excluding the vertical excitation in the analysis significantly underestimates the sliding displacement, particularly for higher friction coefficients.

The ASCE 43-05 and 4-16 approximate method is significantly overconservative for all ranges of μ and for both high and low shaking intensity. The conservativeness may be attributed to the effective friction coefficient which is significantly reduced due to the vertical floor accelerations. While less significant, it is recommended to use the SRSS spatial combination method instead of the 100-40-40 rule to avoid additional conservatism.

The best intensity measure for predicting peak sliding behaviour is dependent on the coefficient of sliding friction. For $\mu < 0.3$, it is advisable to use PFV or other velocity-based measures such as the Fajfar Index. For $\mu > 0.4$, PFA is the most efficient IM. Arias Intensity is also a very efficient measure for mid-range friction coefficients between 0.3 to 0.4. None of these three IMs benefit significantly from including the second horizontal or vertical component of acceleration. Another IM that is comparable in terms of efficiency to Arias Intensity in the high friction range ($\mu > 0.55$) is the dimensionless IM_{12}, but only for the multi-component 2D or 3D cases.

It should be noted that these recommendations are limited in their application due to the specific ground motions and NPP structure used in this paper.

Additional analysis of the sliding response under different earthquake excitation and for different structural periods would give a more complete understanding of the results observed here.

2.13 Acknowledgements

Financial support for the study was provided through the Canadian Nuclear Energy Infrastructure Resilience under Seismic Risk (CaNRisk) – Collaborative Research and Training Experience (CREATE) program of the Natural Science and Engineering Research Council (NSERC) of Canada. The authors are grateful to Dr. Ayman Saudy for providing a STARDYNE 3D stick model of a representative nuclear internal structure. The structural 3D stick model was adapted in OpenSees and analyzed by Mr. Mohammadreza Najafi (MASc Student, McMaster University).

2.14 References

1. *FEMA 74 - Reducing the Risks of Nonstructural Earthquake Damage: A Practical Guide*. vol. 74. 3rd ed. FEMA; 1994.
2. Todd D, Carino N, Chung R, Lew HS, Taylor A, Walton W, *et al. 1994 Northridge Earthquake: Performance of Structures, Lifelines, and Fire Protection Systems*. National Institute of Standards Technology (NIST); .
3. IAEA. *IAEA Mission to Onagawa Nuclear Power Station to Examine the Performance of Systems, Structures and Components Following the Great East Japanese Earthquake and Tsunami*. Onagawa and Tokyo, Japan: 2012.
4. Shenton III HW. Criteria for Initiation of Slide, Rock, and Slide-Rock Rigid-Body Modes. *Journal of Engineering Mechanics* 1996; **122**(7): 690–693. DOI: 10.1061/(ASCE)0733-9399(1996)122:7(690).

5. Newmark NM. Effects of Earthquakes on Dams and Embankments. *Géotechnique* 1965; **15**(2): 139–160. DOI: 10.1680/geot.1965.15.2.139.
6. Choi B, Tung CCD. Estimating Sliding Displacement of an Unanchored Body Subjected to Earthquake Excitation. *Earthquake Spectra* 2002; **18**(4): 601–613. DOI: 10.1193/1.1516750.
7. Kaneko M. Evaluation of Sliding Displacement of Furniture during an Earthquake. *AIJ Journal of Technology and Design* 1999; **5**(8): 73–78. DOI: 10.3130/aijt.5.73.
8. Konstantinidis D, Makris N. Experimental and analytical studies on the response of freestanding laboratory equipment to earthquake shaking. *Earthquake Engineering & Structural Dynamics* 2009; **38**(6): 827–848. DOI: 10.1002/eqe.871.
9. Konstantinidis D, Makris N. Experimental and analytical studies on the response of 1/4-scale models of freestanding laboratory equipment subjected to strong earthquake shaking. *Bulletin of Earthquake Engineering* 2010; **8**(6): 1457–1477. DOI: 10.1007/s10518-010-9192-8.
10. Yeow TZ, MacRae GA, Dhakal RP, Lin SL. Predicting the Maximum Total Sliding Displacement of Contents in Earthquakes. *Journal of Architectural Engineering* 2016; **22**(1): 04015013. DOI: 10.1061/(ASCE)AE.1943-5568.0000193.
11. Konstantinidis D, Nikfar F. Seismic response of sliding equipment and contents in base-isolated buildings subjected to broadband ground motions. *Earthquake Engineering & Structural Dynamics* 2015; **44**(6): 865–887. DOI: 10.1002/eqe.2490.
12. Lopez Garcia D, Soong TT. Sliding fragility of block-type non-structural components. Part 1: Unrestrained components. *Earthquake Engineering & Structural Dynamics* 2003; **32**(1): 111–129. DOI: 10.1002/eqe.217.
13. Chaudhuri SR, Hutchinson TC. Fragility of Bench-Mounted Equipment Considering Uncertain Parameters. *Journal of Structural Engineering* 2006; **132**(6): 884–898. DOI: 10.1061/(ASCE)0733-9445(2006)132:6(884).
14. Nikfar F, Konstantinidis D. Peak Sliding Demands on Unanchored Equipment and Contents in Base-Isolated Buildings under Pulse Excitation. *Journal of Structural Engineering* 2017; **143**(9): 04017086. DOI: 10.1061/(ASCE)ST.1943-541X.0001811.
15. Jangid RS. Seismic response of sliding structures to bidirectional earthquake excitation. *Earthquake Engineering & Structural Dynamics* 1996; **25**(11): 1301–1306. DOI: 10.1002/(SICI)1096-9845(199611)25:11<1301::AID-EQE618>3.0.CO;2-3.

16. Ray Chaudhuri S, Hutchinson TC. Characterizing frictional behavior for use in predicting the seismic response of unattached equipment. *Soil Dynamics and Earthquake Engineering* 2005; **25**(7–10): 591–604. DOI: 10.1016/j.soildyn.2004.11.022.

17. Wen YK. Method for random vibration of hysteretic systems. *Journal of the Engineering Mechanics Division* 1976; **102**(2): 249–263.
18. Park YJ, Wen YK, Ang AHS. Random vibration of hysteretic systems under bi-directional ground motions. *Earthquake Engineering & Structural Dynamics* 1986; **14**(4): 543–557. DOI: 10.1002/eqe.4290140405.
19. Wang CH, Wen YK. Evaluation of Pre-Northridge Low-Rise Steel Buildings. I: Modeling. *Journal of Structural Engineering* 2000; **126**(10): 1160–1168. DOI: 10.1061/(ASCE)0733-9445(2000)126:10(1160).
20. Harvey PS, Gavin HP. Truly isotropic biaxial hysteresis with arbitrary knee sharpness. *Earthquake Engineering & Structural Dynamics* 2014; **43**(13): 2051–2057. DOI: 10.1002/eqe.2436.
21. ASCE. *ASCE 43-05: Seismic Design Criteria for Structures, Systems, and Components in Nuclear Facilities*. Reston, VA: American Society of Civil Engineers; 2005. DOI: 10.1061/9780784407622.
22. ASCE. *ASCE 4-16: Seismic Analysis of Safety-Related Nuclear Structures*. American Society of Civil Engineers; 2017.
23. Nikfar F, Konstantinidis D. Effect of the Stick-Slip Phenomenon on the Sliding Response of Objects Subjected to Pulse Excitation. *Journal of Engineering Mechanics* 2017; **143**(4): 04016122. DOI: 10.1061/(ASCE)EM.1943-7889.0001183.
24. Ma F, Zhang H, Bockstedte A, Foliente GC, Paevere P. Parameter Analysis of the Differential Model of Hysteresis. *Journal of Applied Mechanics* 2004; **71**(3): 342. DOI: 10.1115/1.1668082.
25. Sato E, Furukawa S, Kakehi A, Nakashima M. Full-scale shaking table test for examination of safety and functionality of base-isolated medical facilities. *Earthquake Engineering & Structural Dynamics* 2011; **40**(13): 1435–1453. DOI: 10.1002/eqe.1097.
26. Chaudhuri SR, Hutchinson TC. *Performance Characterization of Bench- and Shelf-Mounted Equipment*. UC Berkley: Pacific Earthquake Engineering Research Center; 2005.

27. Mokha AS, Constantinou MC, Reinhorn AM. Verification of Friction Model of Teflon Bearings under Triaxial Load. *Journal of Structural Engineering* 1993; **119**(1): 240–261. DOI: 10.1061/(ASCE)0733-9445(1993)119:1(240).
28. Huang YN, Whittaker AS, Constantinou MC, Malushte S. Seismic demands on secondary systems in base-isolated nuclear power plants. *Earthquake Engineering & Structural Dynamics* 2007; **36**(12): 1741–1761. DOI: 10.1002/eqe.716.
29. Yu CC, Bolisetti C, Kosbab B, Coleman J. Seismic isolation of a nuclear structure: impacts on construction cost and seismic risk, *Structural Mechanics in Reactor Technology - SMiRT 24*. Busan, South Korea: 2017.
30. Petersen MD, Moschetti MP, Powers PM, Mueller CS, Haller KM, Frankel AD, *et al. Seismic-hazard maps for the conterminous United States, 2014*. Reston, VA: 2015. DOI: 10.3133/sim3325.
31. Brookhaven National Laboratory. *Evaluation of the Seismic Design Criteria in ASCE/SEI Standard 43-05 for Applicaiton to Nuclear Power Plants*. U.S. Nuclear Regulatory Commission (NRC); 2007.
32. Unified Hazard Tool. *USGS*. https://earthquake.usgs.gov/hazards/interactive/ [accessed June 5, 2018].
33. Gülerce Z, Abrahamson NA. Site-Specific Design Spectra for Vertical Ground Motion. *Earthquake Spectra* 2011; **27**(4): 1023–1047. DOI: 10.1193/1.3651317.
34. *Confirmatory Analysis of Seismic Hazard at the Diablo Canyon Power Plant from the Shoreline Fault Zone*. U.S. Nuclear Regulatory Commission; 2012.
35. SCDOT Geotechnical Design Manual - Chapter 12 Geotechnical Earthquake Engineering 2008.
36. FEMA. *FEMA P-1050: NEHRP Recommended Seismic Provisions for New Buildings and Other Structures*. vol. 1: Part 1 Provisions, Part 2 Commentary. FEMA P-1050-1/2015. FEMA; 2015.
37. Kalkan E, Kwong NS. Pros and Cons of Rotating Ground Motion Records to Fault-Normal/Parallel Directions for Response History Analysis of Buildings. *Journal of Structural Engineering* 2014; **140**(3): 04013062. DOI: 10.1061/(ASCE)ST.1943-541X.0000845.
38. Jangid RS. Response of pure-friction sliding structures to bi-directional harmonic ground motion. *Engineering Structures* 1997; **19**(2): 97–104.
39. Taniguchi T, Miwa T. A simple procedure to approximate slip displacement of freestanding rigid body subjected to earthquake motions. *Earthquake Engineering & Structural Dynamics* 2007; **36**(4): 481–501. DOI: 10.1002/eqe.639.

40. Nie J, Morante RJ, Miranda MJ, Braverman JI. On the Correct Application of the 100-40-40 Rule for Combining Responses Due to Three Directions of Earthquake Loading. *ASME 2010 Pressure Vessels and Piping Conference: Volume 8*, *ASME 2010 Pressure Vessels and Piping Division/K-PVP Conference*. Bellevue, Washington, USA: ASME; 2010. DOI: 10.1115/PVP2010-25466.
41. Newmark NM, Hall WJ. *Development of criteria for seismic review of selected nuclear power plants*. United States: 1978.
42. Padgett JE, Nielson BG, DesRoches R. Selection of optimal intensity measures in probabilistic seismic demand models of highway bridge portfolios. *Earthquake Engineering & Structural Dynamics* 2008; **37**(5): 711–725. DOI: 10.1002/eqe.782.
43. Dimitrakopoulos EG, Paraskeva TS. Dimensionless fragility curves for rocking response to near-fault excitations. *Earthquake Engineering & Structural Dynamics* 2015; **44**(12): 2015–2033. DOI: 10.1002/eqe.2571.
44. Theil H, Cramer JS, Moerman H, Russchen A. *Economic Forecasts and Policy*. North-Holland Publishing Company; 1961.
45. Giouvanidis AI, Dimitrakopoulos EG. Rocking amplification and strong-motion duration. *Earthquake Engineering & Structural Dynamics* 2018; **47**(10): 2094–2116. DOI: 10.1002/eqe.3058.
46. O'Hara TF, Jacobson JP (Yankee AEC Bolton, MA (United States)). *Standardization of the cumulative absolute velocity*. United States: Electric Power Research Institute (EPRI); 1991.
47. Kramer SL, Mitchell RA. Ground Motion Intensity Measures for Liquefaction Hazard Evaluation. *Earthquake Spectra* 2006; **22**(2): 413–438. DOI: 10.1193/1.2194970.
48. Arias A. A measure of earthquake intensity. In: Hansen R, editor. *Seismic design for nuclear power plants.*, Cambridge: MIT Press; 1970.
49. Fajfar P, Vidic T, Fischinger M. A measure of earthquake motion capacity to damage medium-period structures. *Soil Dynamics and Earthquake Engineering* 1990; **9**(5): 236–242. DOI: 10.1016/S0267-7261(05)80002-8.
50. Park YJ, Ang A H-S, Wen YK. *Seismic Damage Analysis and Damage-Limiting Design of R.C. Buildings*. University of Illinois; 1984.
51. Wilson R. *Relation of Arias Intensity to Magnitude and Distance in California*. U.S. Department of Interior: U.S. Geological Survey; 1993.
52. Petrone C, Di Sarno L, Magliulo G, Cosenza E. Numerical modelling and fragility assessment of typical freestanding building contents. *Bulletin of*

Earthquake Engineering 2017; **15**(4): 1609–1633. DOI: 10.1007/s10518-016-0034-1.

Chapter 3. Conclusions and Recommendations

3.1 Summary

There is concern that the movement of nonstructural equipment and contents (EC) within nuclear power plants (NPPs) may interact with other systems and components, posing a safety-risk to the facility. In order to better understand and predict this behaviour different analysis cases and intensity measures were studied. First, 20 ground motions histories were selected and scaled to target spectra for locations that experience both low and high seismicity and based on the sites of two currently operating NPPs within the United States. Next, the ground motions were applied to the structural model of a representative nuclear facility to obtain floor acceleration histories which were used as input for the sliding model. The sliding model was based on a biaxial Bouc-Wen type model and the equation of motion for a rigid sliding block. The cases examined were unidirectional (1D), bidirectional (2D), unidirectional and vertical (1D+V), and bidirectional and vertical (2D+V) excitation. For each case, the name implies which acceleration components were applied simultaneously. The peak sliding displacements calculated from the ASCE approximate method as well as the accuracy of the spatial combination rules allowed within the standard were examined in comparison to the 2D+V case from the sliding model. Furthermore, the concept of multi-directional excitation was expanded to intensity measures (IMs). A list of 12 IMs were identified from existing literature and modified to include the x and y

(2D) or *x*, *y* and *z* (3D) components of acceleration. The IMs are compared against the 2D+V peak sliding displacement, which is identified as the engineering demand parameter for all 40 ground motions. Linear regression analysis is conducted, and the coefficient of determination is used to evaluate the efficiency of each intensity measure.

3.2 Recommendations

In Conclusion, the analysis shows that the influence of the bidirectional interaction and vertical component of acceleration is largest for sites with high seismic hazard and more apparent at higher values of μ. The differences between the 1D, 1D+V, 2D, and 2D+V models is more pronounced for sites with high seismic hazard due, in part, to larger sliding displacements from higher-intensity ground motions. The ASCE approximate method is found to be significantly over-conservative. The best intensity measures for predicting sliding displacement are not significantly changed by including multi-component excitation. Detailed conclusions and recommendations for specific friction ranges and seismic hazard levels are given below. It should be noted that these recommendations are limited in their application due to the locations and specific ground motions used in this paper.

At low seismic hazard and for $\mu > 0.4$ it is acceptable to use any model, as they all converge to the same displacement for higher friction coefficients and the difference between displacements for higher friction coefficient is very minimal

(<1mm). For $\mu \leq 0.4$ the 1D analysis case can underestimate the response by a factor of 0.7, which may or may not be a concern depending on the magnitude of displacement observed. Overall, for low shaking intensity sites such as Robinson, the influence of the bidirectional interaction and vertical component of excitation is lower.

At high shaking intensity and for $\mu < 0.2$, the effect of the vertical component is not significant. For $\mu \geq 0.2$ both the 2D and 1D+Vertical follow the same response curve, indicating that the effect of bidirectional interaction and vertical acceleration are similarly unconservative when compared to the 2D+V model. In all cases it is not recommended to use the 1D model since it can underestimate the displacement response by a ratio of 0.87 to 0.66 as the friction coefficient increases.

The approximate method is significantly overconservative regardless of friction and seismic hazard. For lower shaking intensity the method is especially inaccurate for high friction coefficients, overestimating the displacement response by a factor of up to 45 for $\mu > 0.5$.

The best intensity measure for $\mu < 0.3$, is peak floor velocity or the Fajfar Index. For $\mu > 0.3$, peak floor acceleration and Arias intensity are the most efficient IMs, with peak floor acceleration being most efficient at higher friction. None of these IMs benefit significantly from incorporating the second horizontal or vertical component of acceleration.

3.3 Future Research

Additional research may include more detailed investigation of the sliding displacement following the development of a more complex bidirectional frictional model that can capture the Stribeck effect or pre-sliding behaviour, which is verified through experimental validation. The sliding behaviour of the block can be analyzed for other buildings to see if the conclusions from this study can be generalized for any scenario or if they are only valid for stiff (short-period) structures and these specific floor acceleration histories. Following the additional analysis, recommendations for a less over-conservative approximate method or more accurate prediction equations for sliding displacement can be established. Also, the evaluation of intensity measures (IMs) is currently based solely on efficiency but can be expanded to consider other factors. These include practicality (level of correlation between demand parameter and IM based on the slope of the regression line), proficiency (a function of efficiency and practicality) and hazard computability (level of difficulty to compute). The research on IMs can also be furthered to develop fragility curves for sliding displacement of equipment in NPPs.